Received: 2 January 2020 | Revised: 1 February 2020 | Accepted: 8 February 2020

DOI: 10.1002/inf2.12105

REVIEW ARTICLE

WILEY

Addressing the Achilles' heel of pseudocapacitive materials: Long-term stability

Tianyu Liu[1] | **Yat Li**[2]

[1]Department of Chemistry, Virginia Polytechnic Institute and State University, Blacksburg, Virginia

[2]Department of Chemistry and Biochemistry, University of California, Santa Cruz, California

Correspondence
Tianyu Liu, Department of Chemistry, Virginia Polytechnic Institute and State University, Blacksburg, VA 24061.
Email: tliu23@vt.edu
Yat Li, Department of Chemistry and Biochemistry, University of California, Santa Cruz, CA 95064.
Email: yatli@ucsc.edu

Funding information
Merced nAnomaterials Center for Energy and Sensing (MACES), Grant/Award Number: NNX15AQ01

Abstract

Electrode materials with high energy densities and long-lasting performances are crucial to durable and reliable electrochemical energy storage devices for modern information technologies (eg, Internet of things). In terms of supercapacitors, their low energy densities could be enhanced by using pseudocapacitive electrodes, but meanwhile, their ultralong lifetimes are compromised by the limited charge-discharge cycling stabilities of pseudocapacitive materials. This review article discusses on the cycling instability issues of five common pseudocapacitive materials: conjugated polymers (or conducting polymers), metal oxides, metal nitrides, metal carbides, and metal sulfides. Specifically, the article includes the fundamentals of the failure modes of these materials, as well as thoroughly surveys the design rationales and technical details of the cycling-stability-boosting tactics for pseudocapacitive materials that reported in the literature. Additionally, promising opportunities, future challenges, and possible solutions associated with pseudocapacitive materials are discussed.

KEYWORDS

conjugated polymer, cycling stability, metal carbide, metal nitride, metal oxide, metal sulfide, pseudocapacitive

1 | INTRODUCTION

Electrical energy is of paramount importance in the Information Age. Energy storage devices that store, manage, and distribute electrical energy are indispensable for the development of contemporary information technologies, such as smart electronics, the Internet of things (IoTs), and the Internet of everything.[1,2] Among various energy storage devices, supercapacitors, also known as ultracapacitors or electrochemical capacitors, stand out because of their ultrahigh power density and superior durability. Generally, supercapacitors' power densities are ~100 times higher than those of conventional batteries, and supercapacitor devices can last millions of charge-discharge cycles without noticeable capacitance fade.[1,3] Driven by the need to boost the energy densities of supercapacitors, a diverse array of pseudocapacitive electrode materials have been investigated to replace conventional carbon-based electrical double layer capacitive materials, for example, activated carbon. Activated carbon exhibited limited capacitance, particularly at ultrafast charging and discharging rates, due to the dominance of micropores that are poorly ion accessible.[4,5] Pseudocapacitive electrodes, including conducting polymers (or more rigorously speaking, conjugated polymers),[6,7] metal oxides,[8] metal sulfides,[9,10] metal nitrides,[11] and metal carbides,[12,13] are promising materials that could simultaneously achieve high energy density and high power density.[14]

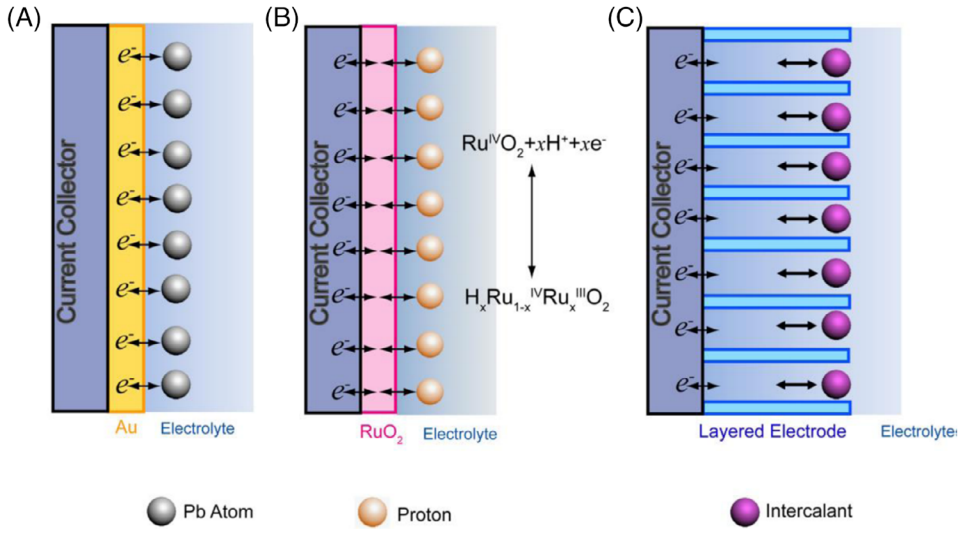

FIGURE 1 Schematic illustrations of three pseudocapacitive reactions: A, underpotential deposition (Pb deposition on Au), B, surface redox reactions (protonation and deprotonation of RuO_2), and C, fast-rate ion intercalation or insertion. Reproduced with permission from Reference 16. Copyright 2017, T.L

The charge-storage mechanisms of pseudocapacitive materials are associated with surface-controlled (kinetically fast), faradaic redox reactions.[14-16] There are three types of pseudocapacitive reactions (Figure 1): underpotential deposition, surface redox reactions, and fast-rate ion intercalation or insertion. Underpotential deposition refers to electrodepositions occurring at potentials less negative than the Nernstian, or thermodynamically equilibrium, potentials (eg, Pb deposition on Au, Figure 1A). The underpotential deposition of hydrogen gas from hydrogen atoms adsorbed on the Pt surface led to the concept of pseudocapacitance in 1962.[17] In the catalysis field, these reactions could evaluate the electrochemically active surface areas of catalysts,[18] but have not yet been applied to energy storage due to their self-limiting nature and limited capacities. Surface redox reactions store charges via chemical reactions involving charge transfer across electrode-electrolyte interfaces (Figure 1B). These processes change the valence states of electrode materials. Hydrous RuO_2 and MnO_2 are two model redox pseudocapacitive compounds. Pseudocapacitive materials storing electrical energy through fast-rate ion intercalation or insertion need to possess ion-conducting channels or layers to host guest ions from electrolytes (Figure 1C). These reactions, unlike those in Li-ion batteries, should not trigger phase transformations during charge-discharge processes. Orthorhombic phase Nb_2O_5 (T-Nb_2O_5),[19] bronze phase TiO_2 [TiO_2(B)],[20] and hexagonal phase WO_3 (h-WO_3)[21] are archetypical intercalation pseudocapacitive materials. Unfortunately, these pseudocapacitive charge-storage processes induce the intrinsic instability of some pseudocapacitive materials, which undermines the durability of supercapacitors, making electrical energy storage unstable and unreliable.

Cycling stability, a metric quantifying how much capacitance retained after certain durations of operation or numbers of charge-discharge cycles, is a critical figure-of-merit for supercapacitor electrodes. Materials with exceptional capacitance and rate capability have almost no practicability if their lifetimes are limited. The widely accepted criteria for the end-of-life of a supercapacitor are defined as the time when 20% capacitance is lost or the internal resistance doubles.[22,23] In laboratories, cyclic voltammetry (CV, Figure 2A) and galvanostatic (or constant-current) charge-discharge (GCD) tests (Figure 2B) are two common methods to evaluate cycling stability. The capacitances of single electrodes and supercapacitors are calculated at cycles with fixed intervals. The percentage of capacitance retained when compared to the begin-of-life (or initial) capacitance is coined capacitance retention and is often used to compare the cycling stability of different materials (Figure 2D). In recent years, researchers proposed methods in addition to CV and GCD, such as voltage hold or potential floating[22,24,25] (Figure 2C), to assess the cycling stability of supercapacitor devices. In these methods, a supercapacitor undergoes three steps per testing cycle: first charged to its maximal potential, dwelled at the peak potential for certain periods, and fully discharged. As each cycle follows the actual working steps of supercapacitors, these methods can provide more realistic results than CV or galvanostatic charge-discharge alone. Industrial protocols on the evaluation of supercapacitor aging are mainly about

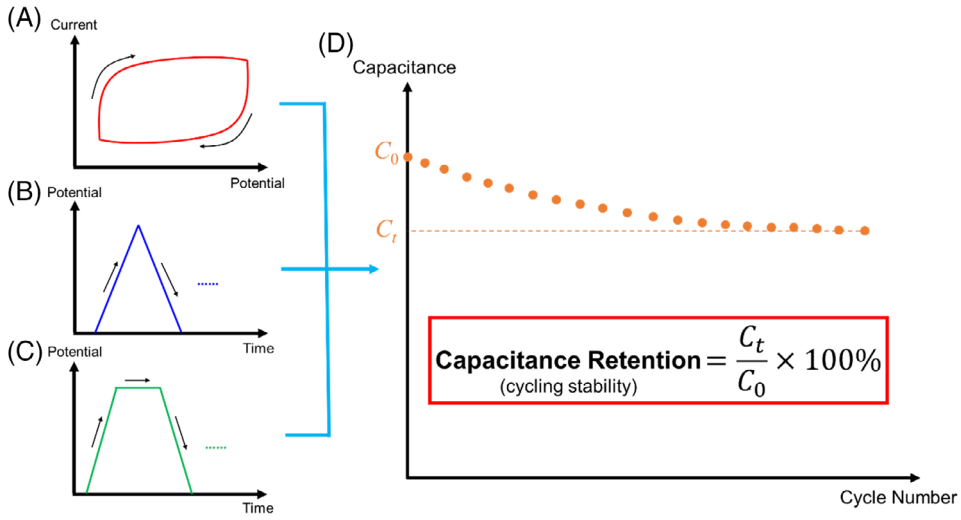

FIGURE 2 A-C, Schemes of cycling stability evaluation methods of, A, cyclic voltammetry, B, galvanostatic (or constant-current) charge–discharge test, and, C, voltage-hold (or potential floating) test. D, An illustration of a typical cycling stability result. The inset shows the mathematical equation of capacitance retention

electrical-double-layer capacitors and involve harsh testing conditions, such as extensively applying high voltages and large currents, to meet the stringent reliability requirements for large-scale, enduring commercial applications.[26,27]

This review article will discuss the recent progress in stabilizing most common pseudocapacitive electrode materials, that is, conjugated polymers, metal oxides, metal nitrides, metal carbides, and metal sulfides. The article begins by summarizing the typical failure modes of these pseudocapacitive electrodes (Section 2), followed by diving into the strategies of curtailing the capacitance-degradation issues (Section 3). Each subsection in Section 3 will start with general descriptions about the latest progress of the corresponding method and then exemplified with one or two representative works. In the last section (Section 4), we will summarize the mechanisms and examples of all the strategies, as well as comment on the challenges and associated opportunities of stabilizing pseudocapacitive materials. We need to point out that the instability of electrode materials is only one of the reasons causing the poor stability of some pseudocapacitors. Other factors that are not directly related to electrodes, such as gel electrolyte solidification or dehydration, electrolyte decomposition, or unsuitable operation temperatures, would also lead to the demise of supercapacitors. However, to keep the article cohesive and coherent, this review will focus only on the stability issues of pseudocapacitive electrode materials, the most common reason for the failure of high-energy-density supercapacitors.

2 | FAILURE MODES OF PSEUDOCAPACITIVE MATERIALS

Their undesirable cycling stability often shadows the inherently large capacitance of pseudocapacitive materials. These drawbacks result from complex factors associated with the structural integrity, electronic properties, and electrochemical behaviors of pseudocapacitive materials.

2.1 | Structure disintegration

Materials store charges through incorporation, insertion, or intercalation of guest species often fail because of structural instability. Similar to battery materials, the uptake and release of guest species accompany expansion and contraction of the host materials, respectively. Such repeated volumetric deformations create internal osmotic stress that cracks, pulverizes, or detaches active materials.

Conjugated polymers are typical pseudocapacitive materials suffering from structure disintegration. Taking polyaniline (PANI) as an example, its charge-storage activity relies on the doping and de-doping of counterions during charge and discharge, respectively (Figure 3). Starting from the undoped leucoemeraldine form, PANI impregnates anions in electrolytes upon oxidation and transits to the partial-doped emeraldine salt, and eventually to the full-doped pernigraniline salt. The neutrality of PANI is maintained by charge balance between the positively charged quaternary nitrogen sites on backbones and the negatively charged anions. The insertion of counterions drags in solvent molecules, which also

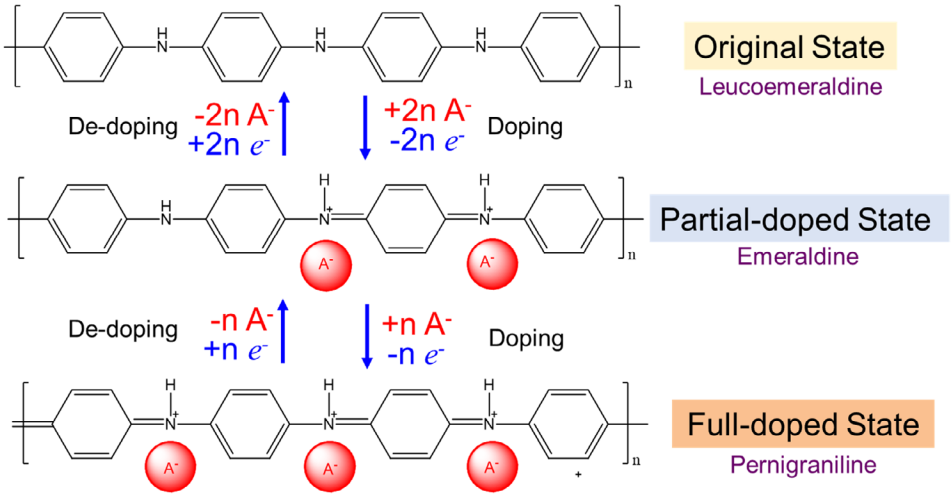

FIGURE 3 Scheme of volumetric change and concurrent molecular structure evolution of polyaniline (PANI) during charge and discharge processes

swells PANI. Volumetric expansion due to the incorporation of ions and solvents is called osmotic expansion. The degree of expansion depends strongly on types and concentrations of the doped ions and counter ions.[28-30] Bay et al quantified the volumetric change of a free-standing dodecylbenzene sulfonate-doped polypyrrole (PPy) thin film in 0.1 to 5.0 M NaCl aqueous electrolytes.[28] In 0.1 M NaCl, the maximal elongation in the lateral direction was 25 $cm^3\ mol^{-1}$ charge. This value decreased to 12 $cm^3\ mol^{-1}$ charge in 5.0 M NaCl due to the reduced water uptake from the aqueous electrolyte. Lizarraga et al studied the volumetric swelling of PANI in protic aqueous solvents including $HClO_4$, H_2SO_4, and HCl. The largest volumetric expansion reached ~6 vol% in 1 M HCl.[31] Although the volumetric expansions of conjugated polymers is less significant than those of some battery electrodes (eg, Si anodes in Li-ion batteries experience ~300 vol% expansion upon full lithiation),[32] the long duration and the repetitive charge-discharge cycles would amplify the destructive force of osmotic expansion and notably degrade the cycling stability. Additionally, intrinsic expansion due to changes in bond lengths and molecular conformations upon ion doping also swells conjugated polymers, but their influence is marginal compared to that of osmotic expansion.[28]

Volumetric deformation is also the direct cause to the structural instability of many metal oxides and metal sulfides, particularly those with layered structures, for example, birnessite-MnO_2 (δ-MnO_2)[33-36] and Co_9S_8.[37] For example, using atomic force microscopy (AFM), Penner and coworkers reported that the diameter of a δ-MnO_2-coated Au nanowire increased from ~120 to ~140 nm (Figure 4A-C).[34] This considerable volumetric expansion cracked the MnO_2 coatings and rapidly decayed the capacitance. For metal sulfides, Su et al used in situ transmission electron microscopy (TEM) technique to record the volumetric expansion of Co_9S_8 during lithiation (Figure 4D-F).[37] After lithiation for 130.75 seconds, the imaged CNT-confined Co_9S_8 nanowire expanded 4.5% axially and 32.4% radially. Although the extent of the volumetric changes of pseudocapacitive metal oxides and sulfides is not as significant as those of battery electrodes, this relatively small internal stress induced by the volumetric deformation, if left undissipated, could accumulate during long-term cycling and become large enough to demolish their structural integrity.

2.2 | Loss of electrical conductivity

Decreasing electrical conductivity of a pseudocapacitive material is detrimental, as it impedes electron transport and deteriorates rate capability. Composition changes due to self-oxidation, overoxidation, and overreduction are the common reasons leading to reduced electrical conductivity of pseudocapacitive materials.

2.2.1 | Metal nitrides

Electrically conductive metal nitrides are promising pseudocapacitive electrodes, but self-oxidation rapidly decreases their capacitance, especially when tested in aqueous electrolytes. Taking TiN as an example, the Pourbaix diagram of Ti-H_2O shows that the most stable Ti species in water with $pH < 14$ is Ti(III) or Ti(IV) oxide.[38] TiN oxidizes in alkaline electrolytes via[39]:

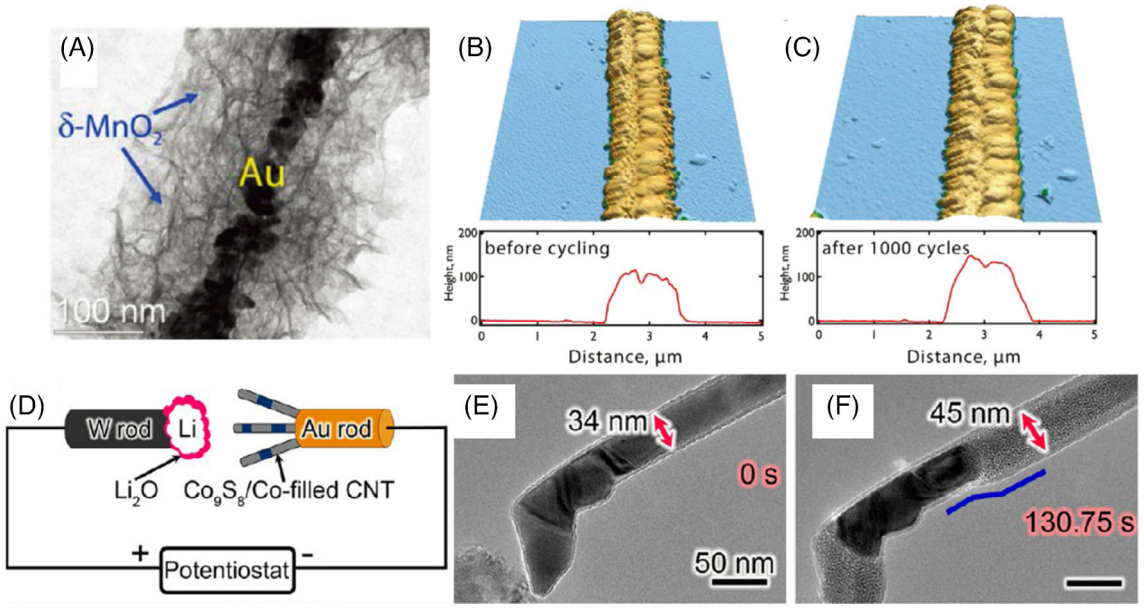

FIGURE 4 (a) Transmission electron microscopy (TEM) image of δ-MnO_2 nanosheets deposited onto a gold nanowire. B,C, Atomic force microscopy (AFM) images of a δ-MnO_2 nanosheets-coated Au nanowire, B, before and, C, after cycling. Cycling conditions: cyclic voltammetry, 100 mV s^{-1}, −0.4 to 0.5 V vs saturated mercurous sulfate. D, Scheme of the setup of an in situ TEM imaging system. E,F, TEM images of a CNT-confined Co_9S_8 nanowire before and after 130.75 seconds of lithiation. Panels A-C: Reproduced with permission from Reference 34. Copyright 2012, The American Chemical Society. Panels D-F: Reproduced with permission from Reference 37. Copyright 2013, The American Chemical Society

$$TiN + 2OH^- + H_2O \leftrightarrow HTiO_3^- + NH_3 \uparrow + e^- \quad (1)$$

or

$$2TiN + 8OH^- \rightarrow 2TiO_2 + N_2 \uparrow + 4H_2O + 8e^- \quad (2)$$

Avasarala and Haldar reported that in acidic media, the oxidation process of TiN is potential dependent.[40] Between 0.5 and ~0.9 V, the reaction is:

$$2TiN + 4H_2O \rightarrow 2TiO_2 + N_2 \uparrow + 8H^+ + 8e^- \quad (3)$$

And between ~1.0 and 1.5 V:

$$TiN + 3H_2O \rightarrow Ti(OH)_3 + N_2 \uparrow + 3H^+ + 3e^- \quad (4)$$

$$2TiN + 6H_2O \rightarrow 2TiO_2 \cdot H_2O + N_2 \uparrow + 8H^+ + 8e^- \quad (5)$$

Besides electrooxidation, TiN can even spontaneously self-oxidize in air at room temperatue[40]:

$$2TiN + 2O_2 \rightarrow TiO_2 + N_2; \Delta G^0 = -611.8\,kJ\,mol^{-1} \quad (6)$$

The presence of Ti—N—O and Ti—O peaks in the Ti 2p X-ray photoelectron spectrum (XPS) and the loss of N signal in the N 1s XPS spectrum (Figure 5)[40-42] are indicators of TiN oxidation. Additionally, Fourier transform infrared spectroscopy (FTIR) can indicate oxidation based on the presence of the —OH stretching peak at ~3050 cm^{-1}.[39]

Oxidation converts highly electrically conductive metal nitrides to semiconducting metal oxides, which increases electrical resistances and impedes fast electron transport. For example, Choi and Kumta observed that the electrical conductivity of TiN nanocrystals decreased from 2662 to 46 S m^{-1} after being charged and discharged for 400 times in a 6 M KOH aqueous electrolyte.[39] The dissolution of the oxidation products in acidic electrolytes drove oxidation throughout TiN and largely diminished its charge-storage capability.

In general, metal compounds having low-valence nonmetal elements, such as MXenes (two-dimensional metal carbides and nitrides)[43-45] and metal sulfides,[46,47] tend to self-oxidize to thermodynamically stable but poorly conductive metal oxides.

2.2.2 | Metal oxides

Oxygen-deficient metal oxides are attractive pseudocapacitive materials because of their enhanced electrical conductivity, augmented charge-carrier mobility, and improved redox activity compared to their stoichiometric

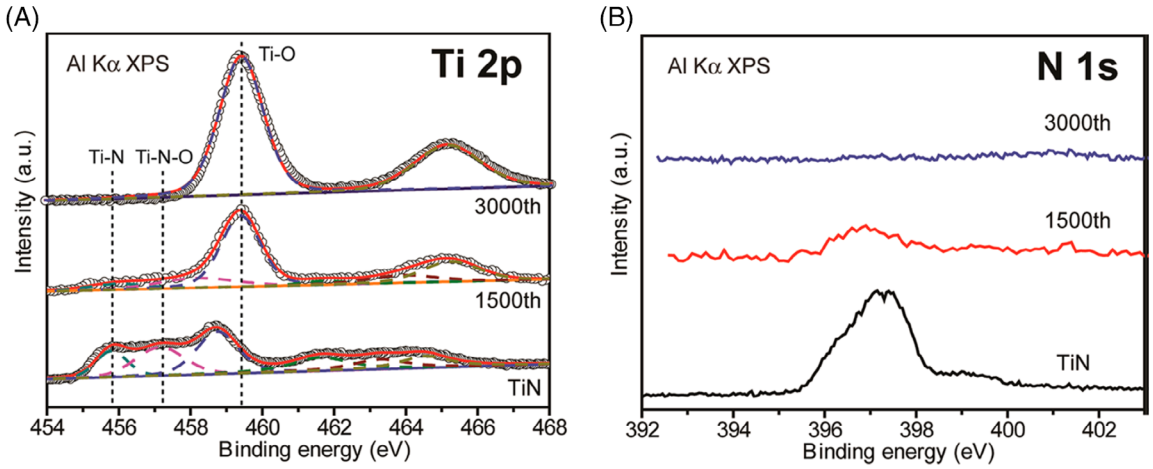

FIGURE 5 Core-level, A, Ti 2p and, B, N 1s XPS spectra of TiN nanowires cycled in an 1 M aqueous KOH electrolyte between −1.0 and 0 V vs Ag/AgCl after different cycles. Reproduced with permission from Reference 42. Copyright 2012, The American Chemical Society

counterparts. However, using nonstoichiometric metal oxides as charge storage media in an improper potential window may lose oxygen defects, reduce electrical conductivities, and inhibit the charge transport. For example, molybdenum oxide (MoO_x) with Mo^{4+} and Mo^{5+} has higher electrical conductivities than MoO_3 (Mo^{6+}).[48] Cycling MoO_x in a potential window between −1.0 and 0 V vs SCE reduced the oxygen nonstoichiometry due to oxidation of Mo^{4+} and Mo^{5+} to Mo^{6+}. This process augmented the electrical resistance and decreased the charge-carrier mobility of MoO_x, which led to over 25% capacitance decay after only 500 charge-discharge cycles.

2.2.3 | Conjugated polymers

The counterion drain effect gradually degrades the electrical conductivity of conjugated polymers. This problem is related to the repeated swell-shrinkage of conjugated polymers that collapses ion diffusion channels and retards doping of ions from electrolytes. This consequence reduces the population of bipolarons, that is, positive charged sites on the backbones of conjugated polymers that conduct electrons,[49-51] and deactivates conjugated polymers.

Additionally, charging conjugated polymers to potentials higher than the upper limits of their potential windows could permanently damage the electrochemical activities of conjugated polymers. This process is called overoxidation and was extensively studied in the 1980s and 1990s. In 1982, Bard and coworkers reported that polypyrrole films "were unstable to oxidative conditions such as potentials >0.6 V vs SCE or the presence of halogens."[52] Others have observed the similar phenomena in the following years.[53-57] The mechanism of overoxidation and its influence on the structure-electrical conductivity relationship are complex and polymer dependent,[50] and calls for continuing investigations. The net outcome of overoxidation, however, is identical to the counterion drain effect: reducing the electrical conductivities of conjugated polymers and making them electrochemically inert.

2.3 | Dissolution of active components

Formation of highly soluble species in electrolytes during charge storage could break the reversibility of electrodes' redox reactions and consume active materials. For example, scanning MnO_2 at potentials below its stable potential window irreversibly reduces MnO_2 to low-valence products, for example, Mn_2O_3 or MnOOH, which undergo disproportionation and yield Mn^{2+} ions.[58,59] Specifically, the dissolution reaction in acidic electrolytes is:

$$Mn_2O_3 + 2H^+ \rightarrow Mn^{2+} + MnO_2 + H_2O \quad (7)$$

In alkaline electrolytes:

$$2MnOOH \rightarrow Mn^{2+} + MnO_2 + 2OH^- \quad (8)$$

Hsieh et al argued the validity of Equations (7) and (8) because they believed that the Mn^{2+} concentration in electrolytes was too small to account for the capacitance loss.[60] This discrepancy was explained by Nam et al who utilized Mn K-edge X-ray near-edge absorption spectroscopy and concluded that the irreversible reduction of MnO_2 proceeded not only near its surface but also in bulk.[61] Additionally, Ataherian et al systematically investigated the interplays among the valence, morphology,

and electrochemical performance of MnO_2.[59] Their experimental results confirmed the relationship between Mn valence reduction and surface morphology reconstruction. The morphological change indicated that MnO_2 experienced a dissolution-recrystallization process during the reduction process. The dissolution, however, was self-limiting because the mixed-valence nature of MnO_x surface halted the continuous dissolution of low-valent manganese oxides and hydroxides.

For metal nitrides and carbides, dissolution could also be triggered by oxidation. For example, V_2O_5 and V_2O_3, the main oxidation products of VN, are readily soluble in acidic aqueous media.[62] The combined loss of electrical conductivity and active materials of VN resulting from oxidation rapidly deteriorate its cycling stability. Besides metal nitrides, Messner et al demonstrated that various metal carbides are also electrochemically oxidizable at potentials higher than 1.0 V vs Ag/AgCl in aqueous electrolytes at various pH values.[63] The metal and carbon elements in these metal carbides were oxidized to corresponding water-soluble metal salts and carbide-derived carbon, respectively.

2.4 | Gas evolution

Gas evolution is a generic adverse event for the cycling stability of all the pseudocapacitor electrodes. When the operation potential exceeds the stable potential thresholds of electrolytes, gas bubbles (eg, hydrogen and oxygen gases) evolve on surfaces of positive and/or negative electrodes due to water electrolysis. Vigorous gas evolution could destruct electrode-current collector interfaces, delaminate active materials from substrates, create pinholes and gaps that increase contact resistance, raise IR drop, decrease coulombic efficiency, and impose safety concerns of joule heating.[64-66] Particularly, gas generation is detrimental to sealed pseudocapacitors because it not only consumes the limited electrolytes but also balloons device pouches that may eventually lead to explosions.

For MnO_2, Ataherian and Wu observed that oxygen evolution at potentials more than 1.0 V vs Ag/AgCl (saturated KCl) reduced Mn^{4+} to Mn^{3+} and Mn^{2+} via a pathway shown in Figure 6.[67] Such irreversible reaction decreased the population of active Mn^{4+} species and lowered the capacitance of MnO_2.

Determining the stable operating potential windows of electrolytes and electrodes before any electrochemical tests is an effective way to avoid gas evolution problems. In CV, steep increase or decrease in current at potential-window limits indicates gas evolution. To prevent such destructive processes, the potential windows must be narrowed. Technical details on deciding suitable potential windows are out of this review's scope, but are available in a recently published perspective article.[68]

3 | STRATEGIES FOR ENHANCING THE CYCLING STABILITY OF PSEUDOCAPACITIVE MATERIALS

This section thoroughly surveys the current progress in the strategies aiming at enhancing the cycling stability of pseudocapacitive materials. The discussion is segmented according to the type of materials: conjugated polymers, metal oxides, metal nitrides, and carbides, as well as metal sulfides. Each subsection is elaborated with specific strategies and exemplified with one or two representative examples. Metal nitrides and carbides are combined because they suffer from the same problem of oxidation.

3.1 | Conjugated polymers

3.1.1 | Spatial confinement

Compounding conjugated polymers with mechanically soft materials is the most widely practiced method to address the structural disintegration of conjugated polymers. These materials function as buffer or cushion substrates that release the stress built in conjugated polymers. Even if the incorporated conjugated polymers crack, the broken pieces could still anchor on the substrates without complete disintegration. Among various host materials, carbon materials are most popular because of their abundance, soft nature, and versatile morphologies. Specifically, porous carbon particles,[69,70] carbon nanotubes,[71-79] reduced graphene oxide (rGO) sheets,[77,78,80-91] graphene oxide,[92] graphite foils,[93] etched carbon fibers,[94] and carbon aerogels[95] are reported carbon hosts. Graphene analogs with layered structures that can accommodate large volumetric expansion, such as molybdenum disulfide (MoS_2),[96,97] black phosphorus,[98] and two-dimensional transition metal nitrides and carbides (MXenes)[99] are also potent candidates for stabilizing conjugated polymers. Surface modifications, including sulfonation,[79] are performed to introduce hydrophilic functionalities that can form covalent bonds and/or hydrogen bonds with conjugated polymers and strengthen their interfaces.

Gogotsi and coworkers demonstrated that $Ti_3C_2T_x$ (T_x represents the terminal functional groups on the Ti—C layers), a compound of MXene, appreciably improved the cycling stability of polypyrrole (PPy).[99] Utilizing the hydrophilic functional groups on the surface of $Ti_3C_2T_x$, the researchers in situ polymerized pyrrole intercalating

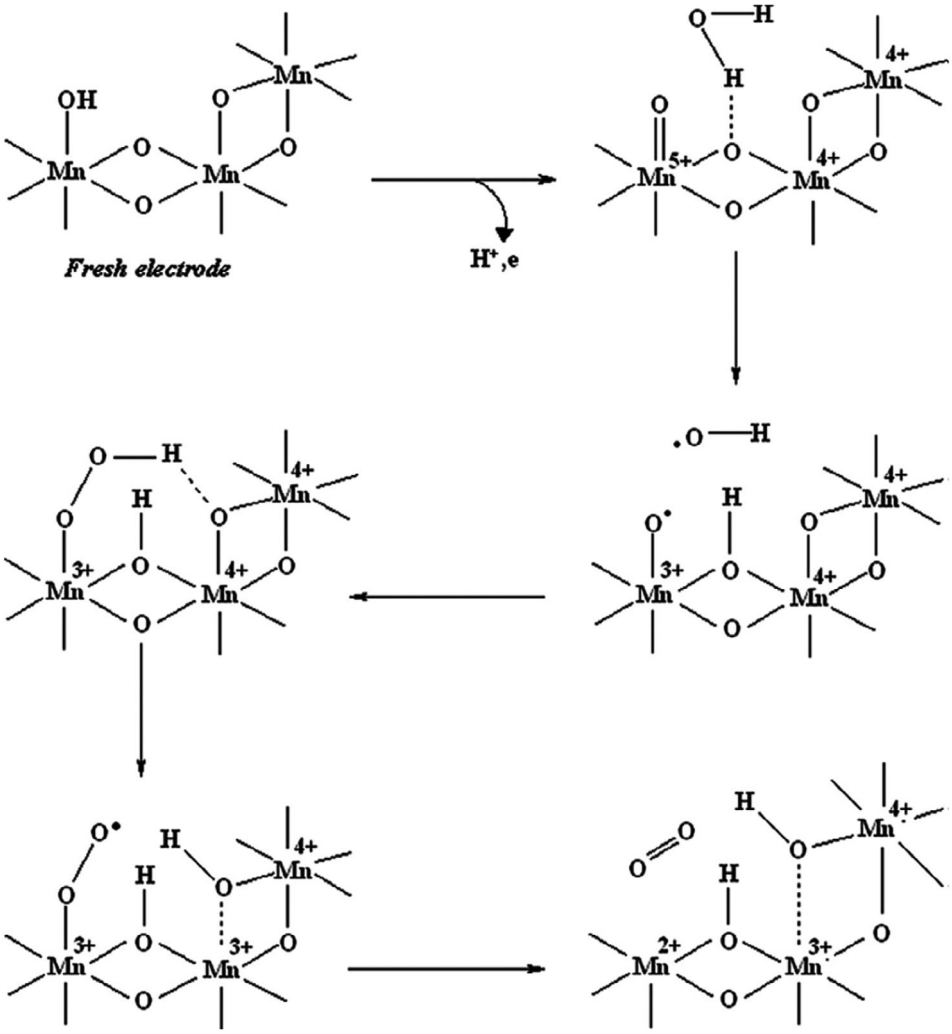

FIGURE 6 A possible mechanism of the oxygen-evolution-induced surface reduction of MnO_2. Reproduced with permission from Reference 67. Copyright 2011, The Electrochemical Society

in the $Ti_3C_2T_x$ layers (Figure 7A). The laminated structure of $Ti_3C_2T_x$ was well preserved after the polymerization, as evidenced by scanning electron microscopy (SEM, Figure 7B) and the periodic pattern under TEM (Figure 7C). Due to the electrochemical activity of PPy, the PPy/$Ti_3C_2T_x$ composite film exhibited capacitances 1.5 to 2.5 times higher than those of bare $Ti_3C_2T_x$ electrodes across a wide range of scan rates (Figure 7D) and ~92% capacitance retention after 25 000 charge-discharge cycles (Figure 7E).

3.1.2 | Surface coating

Compositing conjugated polymers might offer limited protection for nanostructured conjugated polymers with irregularly shaped surfaces, because achieving conformal coverage is challenging. Therefore, conformal coating or encapsulation are strategies to protect nanostructured conjugated polymers. In general, most coating materials are rigid, for example, metal oxides (RuO_2[100] and TiO_2[101]) and Nafion,[102] to withstand the large volumetric expansions of conjugated polymers. Soft and elastic carbon-based materials have also been used as binders to hold the structure of conjugated polymers.[103,104]

One representative example of soft coating materials is glucose-derived carbonaceous shell.[103] Glucose was charred hydrothermally and conformally deposited ~5-nm-thick carbonaceous shells onto PANI and PPy nanowires (PANI@C and PPy@C) (Figure 8A,B). With this coating to strengthen their structural integrity, PANI@C and PPy@C retained ~95% and ~85% of their initial capacitance after 10 000 charge-discharge cycles in 1 M H_2SO_4 aqueous electrolytes, respectively (Figure 8C, D). These stability performances were among the best of conjugated polymers. In comparison, the capacitance of the unprotected PANI and PPy nanowires both dropped to ~20% capacitance at the end of the cycling test.

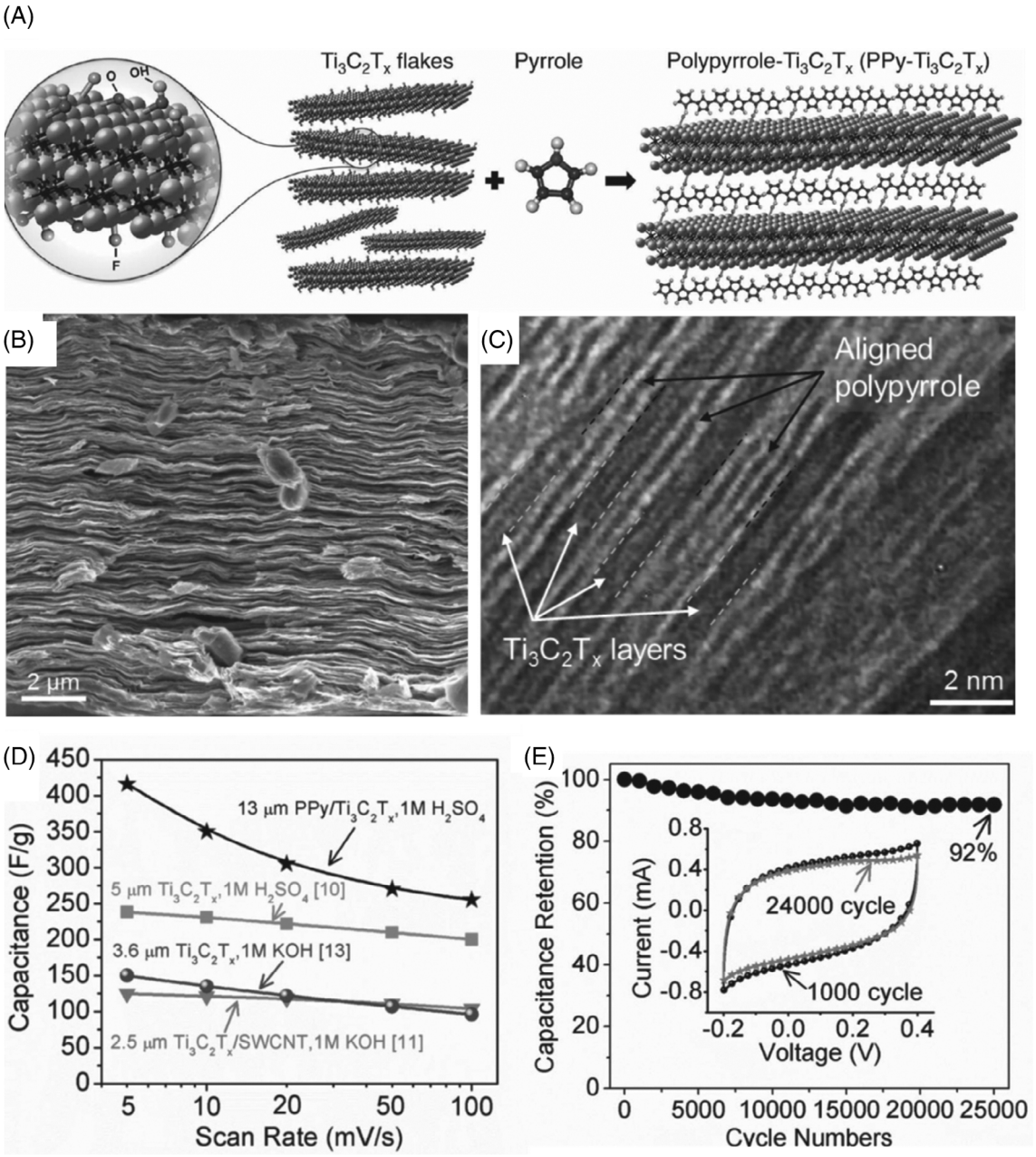

FIGURE 7 $Ti_3C_2T_x$ confinement stabilizes polypyrrole films. A, Scheme of the in situ polymerization of polypyrrole (PPy) among $Ti_3C_2T_x$ nanosheets. B, Scanning electron microscopy (SEM) and, C, transmission electron microscopy (TEM) images of $Ti_3C_2T_x$-confined polypyrrole films (PPy/$Ti_3C_2T_x$). D, Rate capability of PPy/$Ti_3C_2T_x$ in comparison with other $Ti_3C_2T_x$ electrodes. E, Cycling stability of PPy/$Ti_3C_2T_x$ in 1 M H_2SO_4 aqueous electrolyte. Inset: cyclic voltammograms of PPy/$Ti_3C_2T_x$ at the 1000th and 24000th cycles. Reproduced with permission from Reference 99. Copyright 2016, WILEY-VCH Verlag GmbH & Co

Moreover, the cycling stability enhancement was at little cost of capacitance, as evident from the nearly overlapped cyclic voltammograms between the uncoated and coated nanowires (insets of Figure 8C,D). SEM proved that both PANI@C and PPy@C nanowires were preserved after cycling, while all the bare PANI and PPy nanowires disappeared. This discrepancy suggested that the carbon layer effectively suppressed the structure disintegration of PANI and PPy.

3.1.3 | Engineering structures

Engineering structures stabilize conjugated polymers without compounding with other materials. The voids or empty spaces, such as inter-wire gaps of nanowire arrays,[105] hollow chambers of nanotubes,[87,106,107] and pores within three-dimensional architectures[108] buffer volumetric expansions. Sometimes, gel electrolytes are filled in these spaces to provide additional

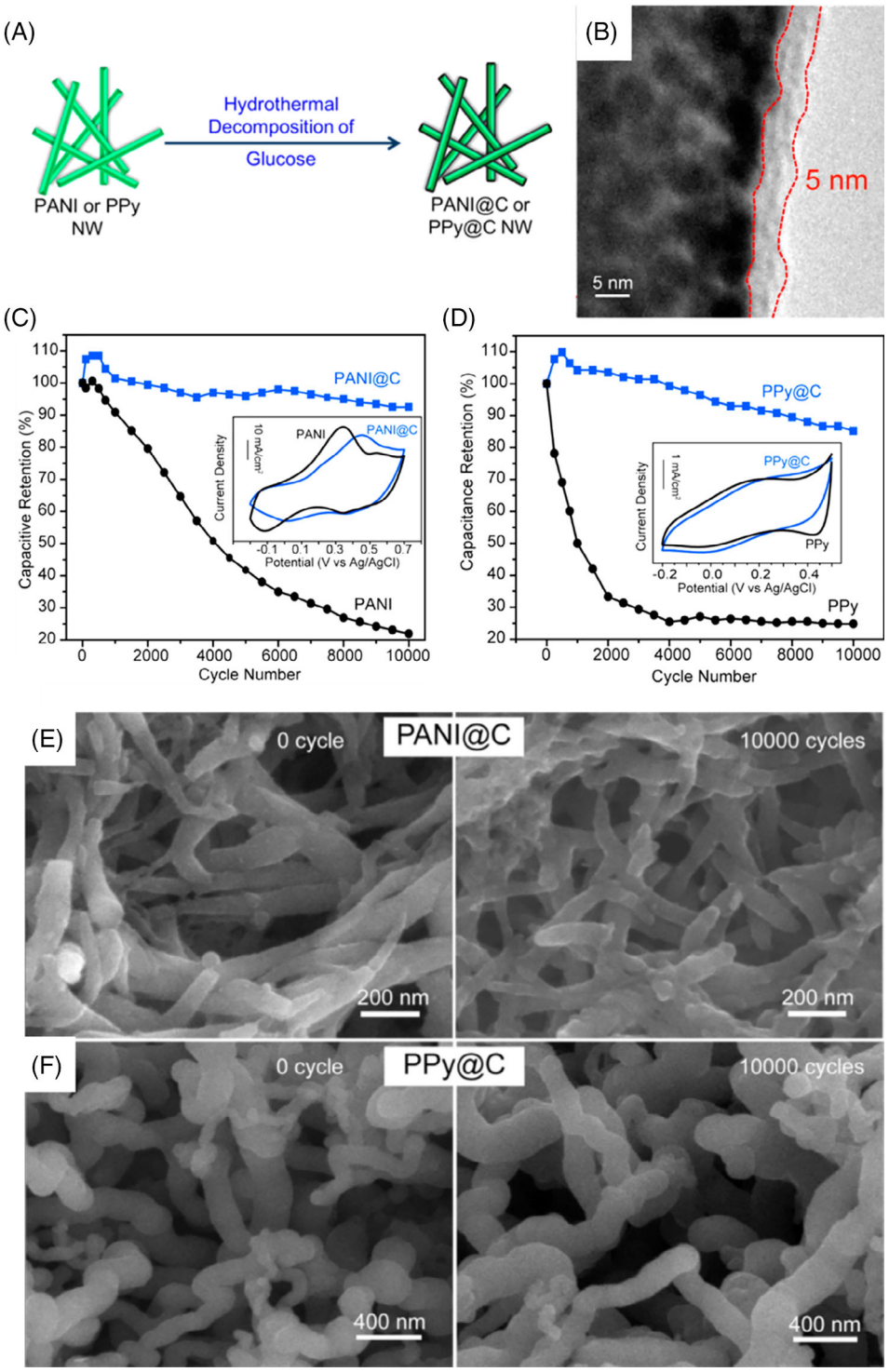

FIGURE 8 Glucose-derived carbonaceous coating stabilizes polyaniline (PANI) and polypyrrole (PPy) nanowires. A, Scheme of a glucose-assisted hydrothermal reaction of depositing thin carbonaceous layers onto PANI and PPy nanowires. B, Transmission electron microscopy (TEM) image of a coated polymer nanowire. The nanowire was sputtered with Au nanoparticles to enhance the contrast between the polymer and its coating. C,D, Cycling stability performance of, C, PANI and PANI@C, and, D, PPy and PPy@C in 1 M aqueous H_2SO_4 electrolytes. E,F, Scanning electron microscopy (SEM) images of, E, PANI@C and, F, PPy@C before and after the cycling stability test. Reproduced with permission from Reference 103. Copyright 2014, The American Chemical Society

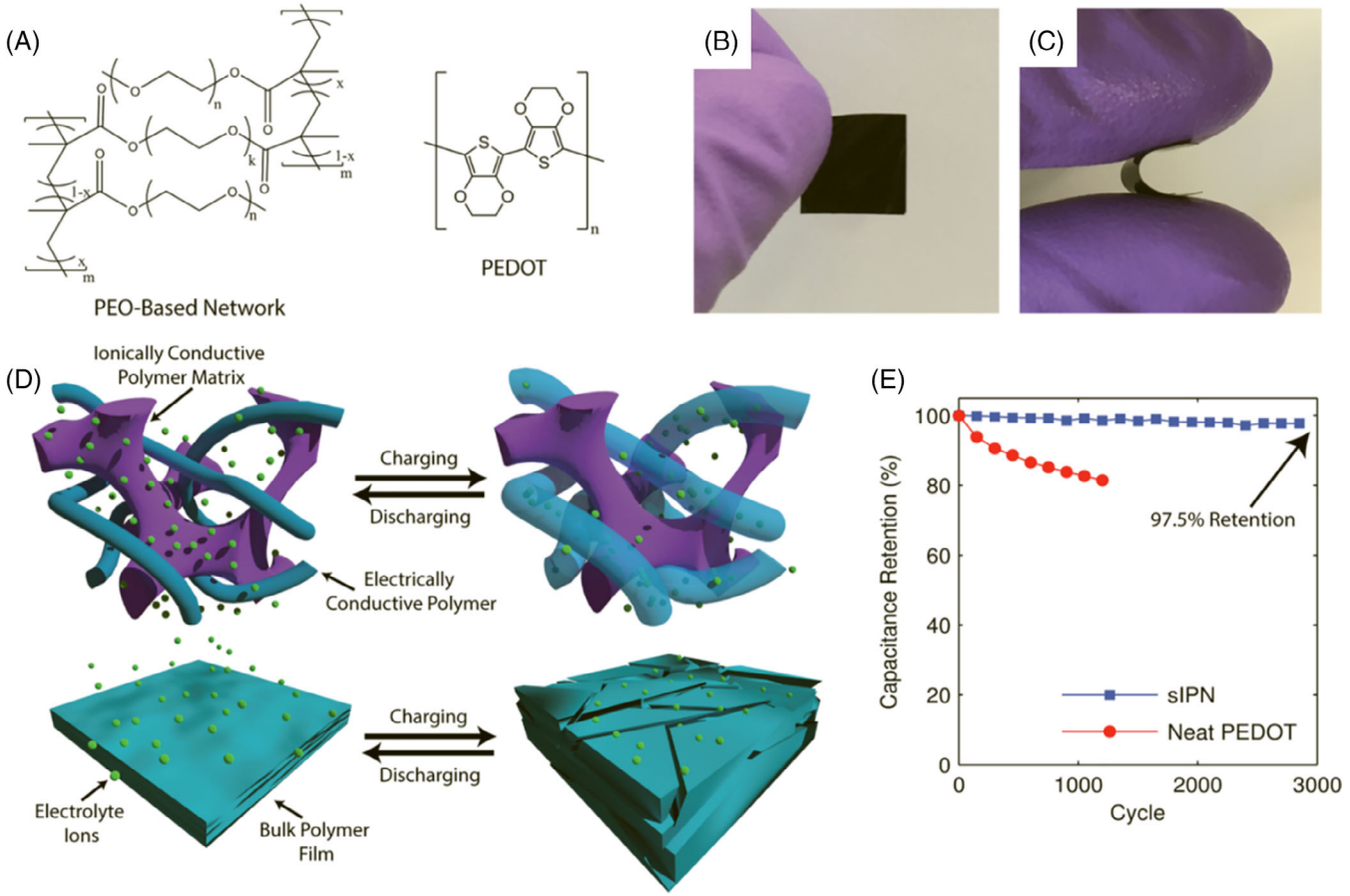

FIGURE 9 Building interpenetrated fiber networks stabilizes poly(3,4-ethylenedioxythiopene) (PEDOT) nanowires. A, Chemical structures of poly(ethylene oxide) (PEO)-based network and PEDOT. B, A piece of self-standing PEDOT/PEO and, C, its flexibility. D, Structure evolutions of interpenetrated PEDOT/PEO networks (SIPN) and neat PEDOT films during extensive charge–discharge cycling. E, Cycling stability of SIPN and neat PEDOT in 1 M $LiClO_4$ organic electrolytes. Reproduced with permission from Reference 109. Copyright 2017, The American Chemical Society

protection and shorten ion diffusion distances.[109] Conjugated polymers are mainly produced by electropolymerization or chemical polymerization with limited controllability on their morphologies. Therefore, nanostructured conjugated polymers usually need hard templates for synthesis.

Smoukov and coworkers demonstrated an excellent example of an interpenetrating nanowire network to stabilize poly(3,4-ethylenedioxythiopene) (PEDOT) nanowires.[109] Using sequential polymerization, the researchers synthesized self-standing poly(ethylene oxide) (PEO)/PEDOT films consisting of interpenetrated PEO and PEDOT nanowires (Figure 9A-C). PEO was percolated with $LiClO_4$ to serve as an ion reservoir, and PEDOT conducted electrons (Figure 9D). The configuration of soft PEO-wrapped PEDOT was helpful in uniformly dissipating the internal stress built in the charged PEDOT nanowires to enhance the cycling stability of PEDOT. The capacitance of PEO/PEDOT retained 97.5% after 3000 cycles at 10 A g^{-1}, whereas that of neat PEDOT continuously decreased within the first 1200 cycles under identical testing conditions (Figure 9E).

3.1.4 | Ordering molecular structures

Configuring molecular structure is effective in minimizing the structural breakdown of PPy. For example, Zhi and coworkers showed that PPy films with a planar molecular configuration displayed outstanding cycling stability.[32] Specifically, the authors compared two types of PPy films synthesized by different methods. One was e-PPy films produced via constant-current electrodeposition in aqueous solutions containing 0.1 M *p*-toluenesulfonic acid, 0.3 M sodium toluenesulfate, and 0.5 vol% pyrrole at 0°C. The aligned electric field favored the deprotonation of pyrrole at its α-position, leading to PPy with a planar configuration (Figure 10A). Another one is c-PPy synthesized by chemical polymerization in

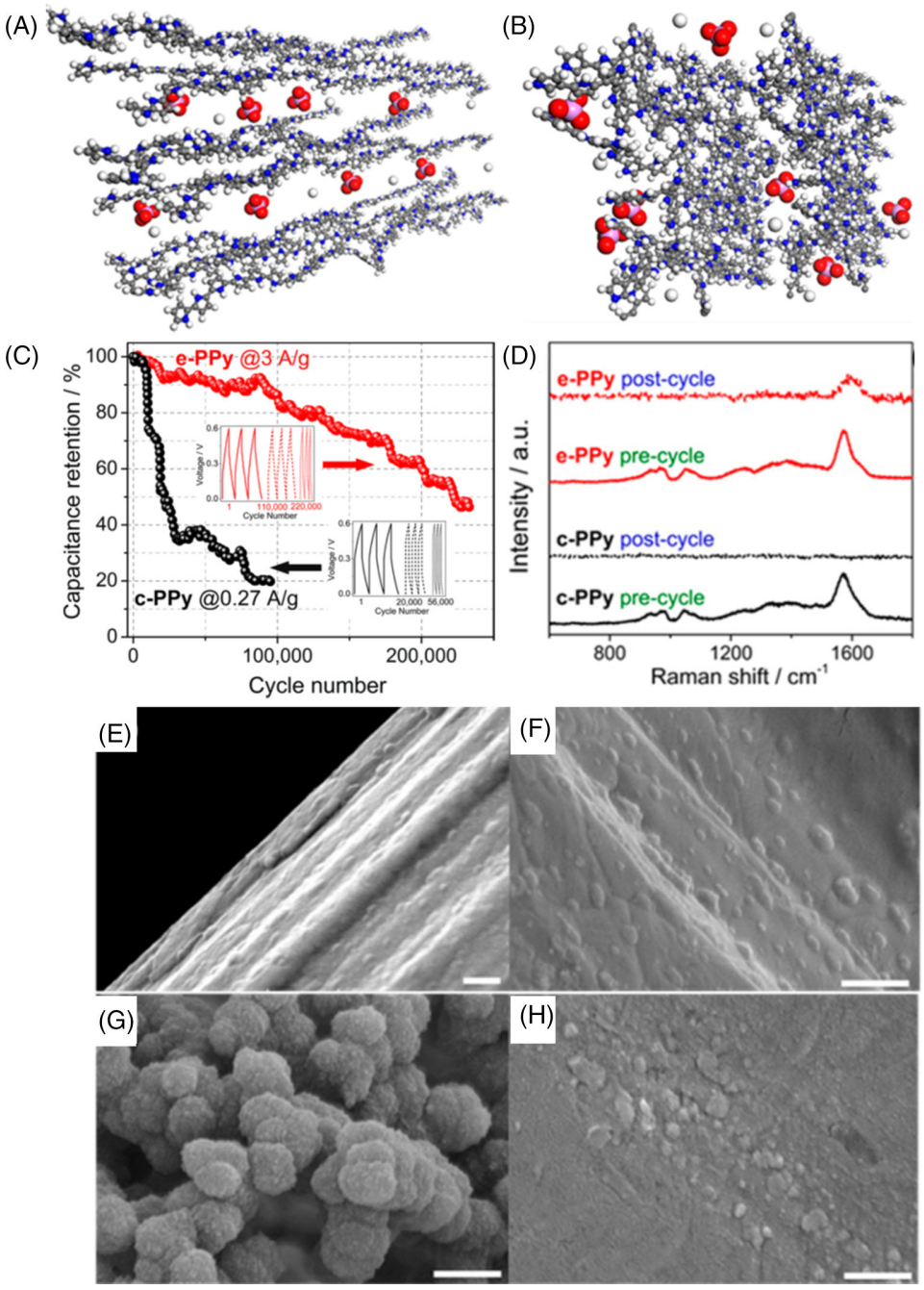

FIGURE 10 Ordering molecular structure stabilizes polypyrrole (PPy) films. A,B, The molecular structures of, A, electrically polymerized PPy (e-PPy) and, B, chemically polymerized PPy (c-PPy). C, Cycling stability of e-PPy and c-PPy in poly(vinyl alcohol) (PVA)/H_3PO_4 gel electrolytes (two-electrode configuration). D, Raman spectra of e-PPy and c-PPy before and after cycling. E-H, Scanning electron microscopy (SEM) images of PPy, E,G, before and, F,H, after cycling: E,F, e-PPy, F,G, c-PPy. Scale bars: 500 nm. Reproduced with permission from Reference 32. Copyright 2016, The American Chemical Society

0.1 M *p*-toluenesulfonic acid and ferric chloride aqueous solutions. The homogeneous oxidized environment of Fe^{3+} had no directing effect for the growth of pyrrole, thus resulted in anisotropic PPy chains (Figure 10B).

Constant-current cycling stability test revealed that e-PPy and c-PPy exhibited drastically different behaviors. The capacitance of c-PPy lost more than 50% after only 1000 cycles (Figure 10C), while that of e-PPy retained >97% after 15 000 cycles. More significantly, the latter retained ~50% capacitance after more than 230 000 cycles.

To understand the origin of the different cycling stability, the authors characterized the morphologies of the two electrodes after the test. Raman spectroscopy showed that the peak at 1573 cm^{-1}, corresponding to C—C

stretching of pyridine rings in PPy, vanished in the spectrum of c-PPy after the cycling test (Figure 10D). This result indicated that the structure of c-PPy was deconstructed at the end of cycling. The C—C stretching Raman peak of e-PPy, in contrast, was still discernible after cycling, meaning its molecular arrangement was preserved. The SEM images showed that the surface morphology of e-PPy changed little after cycling (Figure 10E, F), while the nanospheres of c-PPy disappeared (Figure 10G,H). The enhanced structural integrity of e-PPy was attributed to its planar molecular structure, which uniformly distributed osmotic stress across the entire PPy planes and prevented local-stress-induced damage. The effect of molecular ordering in stabilizing PPy was later acknowledged by Zhou and coworkers.[110]

3.1.5 | Tuning composition

As discussed in Section 2.2.3, the counterion drain effect gradually depletes the dopants in conjugated polymers, making them electrically insulating. While stabilizing the structures of conjugated polymers is useful to maintain their ion diffusion channels, a more direct method to minimize the counterion drain effect is to dope conjugated polymers with immobile anions, such as β-naphthalene sulfonate,[49] sulfanilic acid azochromotrop,[111] *p*-toluenesulfonate,[112] perchlorate,[113] and Tiron,[114] or with bulky redox-active molecules including hydroquinone-benzoquinone.[115,116] The substantial steric hindrance among the polymer chains immobilizes these ionic dopants inside the polymer networks. During charge and discharge, these anions could stay near the polarons without leaking out. Moreover, these bulky anions support ion-diffusion channels and allow for reversible doping and de-doping of small anions from electrolytes, which maintains the charge-storage capacities of conjugated polymers.

A typical example of bulky counterion is β-naphthalene sulfonate anion (NS^-).[49] Compared to sulfate anion, the large naphthalene ring of NS^- significantly restricted its movement among PPy chains. The cycling stability test showed that sulfate anion-doped PPy films on graphite foils exhibited the poorest stability: its capacitance decayed to ~50% after 2000 cycles (Figure 11A, PPy-S). Sulfate-containing PPy films on exfoliated graphite foils exhibited capacitance retention of ~90% after 10 000 cycles, because the graphene layers atop the exfoliated graphite foils served as mechanical buffers to accommodate the volumetric deformation of PPy (Figure 11A, FEG/PPy-S). Remarkably, when doping NS^- into PPy films on exfoliated graphite foils, its cycling stability further improved to 97% after 10 000 cycles (Figure 11A, FEG/PPy-NS). SEM showed that the film morphology of the NS^--doped PPy was intact after cycling (Figure 11B). More importantly, EDS showed that the S signal of NS^- almost unchanged after the stability test, whereas that of sulfonate anion completely disappeared (Figure 11C,D). This observation unequivocally proved that the NS^- stayed in PPy during cycling, which suppressed the counterion drain effect and promoted long lifetimes of PPy electrodes.

3.2 | Metal oxides

3.2.1 | Constructing carbon-based composites

Combining metal oxides with carbon materials simultaneously addresses the oxides' low electrical conductivity and structural instability. First, carbon matrices provide electrons fast diffusion pathways in the metal oxide/carbon composites. Second, the softness of carbon substrates can buffer the volumetric change of metal oxides during charge and discharge. To date, carbon materials of various dimensions, including zero-dimensional carbon dots,[117,118] one-dimensional carbon fibers[119] and carbon nanotubes,[120-126] two-dimensional graphene or rGO sheets,[127-136] three-dimensional porous carbon networks[137] have been combined with metal oxides. Additionally, carbon[138,139] and TiN[140] coatings on metal oxides also stabilize the structure of metal oxides.

Guan et al demonstrated three-dimensional, graphene foam-supported carbon nanotube forests as soft substrates for loading Fe_2O_3 nanoparticles.[120] The CNTs and Fe_2O_3 particles were grown by chemical vapor deposition and atomic layer deposition (ALD), respectively (Figure 12A). SEM (Figure 12B) and TEM images (Figure 12C) both showed that Fe_2O_3 nanoparticles distributed uniformly on the outer surfaces of CNTs. Specifically, CNTs with Fe_2O_3 deposited by 600 ALD cycles (GF-CNT@600-Fe_2O_3) showed cycling stability of 86.2% over 50 000 charge-discharge cycles in 2 M aqueous KOH electrolytes (Figure 12D). This stability outperformed most other Fe_2O_3-based composite electrodes, which was ascribed to the strong bonding between Fe_2O_3 nanoparticles and CNTs, the highly reversible redox reactions of the ultra-small Fe_2O_3 crystals, and the cushion space among the Fe_2O_3 nanocrystals. The initial capacitance decay might correlate to the partial aggregation of the Fe_2O_3 nanoparticles (Figure 12E) that reduced the electrolyte-accessible surface area for redox reactions.

3.2.2 | Tailoring morphology

The structural instability of metal oxides has been partially addressed by building unique nanostructures. The

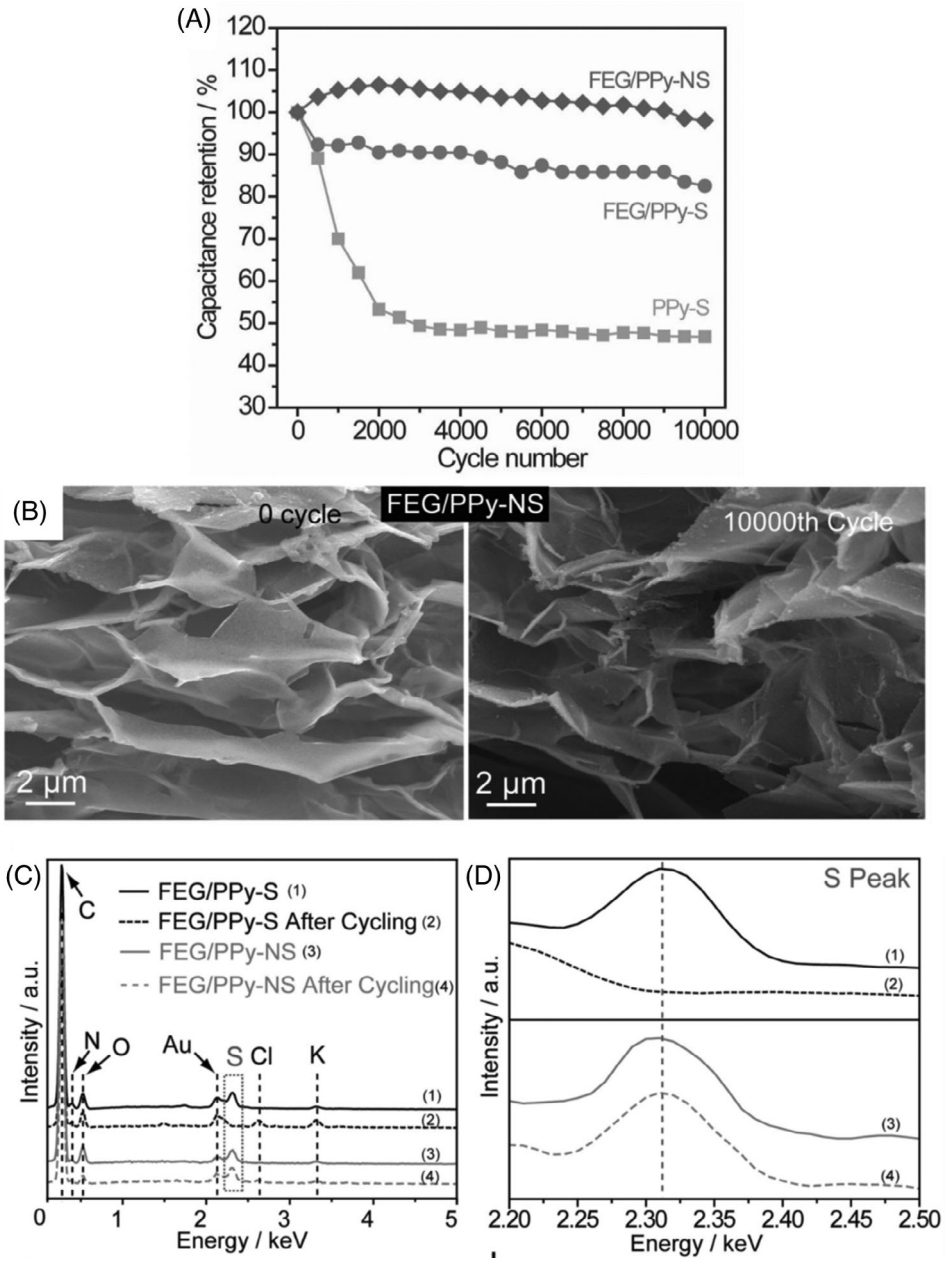

FIGURE 11 Doping immobile counterions stabilizes polypyrrole (PPy). A, Cycling stability of FEG/PPy-NS, FEG/PPy-S, and PPy-S in 3 M aqueous KCl electrolytes. B, Scanning electron microscopy (SEM) of FEG/PPy-NS before and after the cycling stability test. C, EDS survey spectra and, D, the S peak of FEG/PPy-NS and FEG/PPy-S before and after cycling. Reproduced with permission from Reference 49. Copyright 2015, WILEY-VCH Verlag GmbH & Co

stabilization mechanism is identical to that of the nanostructured conjugated polymers (Section 3.1.4). The excellent structural tunability of metal oxides enabled the preparation of nanostructures without hard templates. Nanowires,[141-143] nano-needles,[144] nanosheets,[143-147] and nanorods[148] are morphologies showing improved cycling stability compared to films. Nevertheless, nanostructures alone cannot resolve the dissolution of some metal oxides.

One representative example of how morphology influences the cycling stability of metal oxides was demonstrated by Ouyang et al.[144] Using cetyl trimethyl ammonium bromide and NH_4F as structure-directing agents, the authors synthesized $NiCo_2O_4$ nano-needles ($CC/NiCo_2O_4$-N) and nano-slices ($CC/NiCo_2O_4$-S) on commercial carbon fibers, respectively (Figure 13A). They then deposited NiO nanoflakes onto the nano-needles and nano-slices, forming hierarchical structured $CC/NiCo_2O_4$-N@NiO and $CC/NiCo_2O_4$-S@NiO electrodes. The large volumetric deformation of $NiCo_2O_4$ degraded the cycling stability of $CC/NiCo_2O_4$-S and

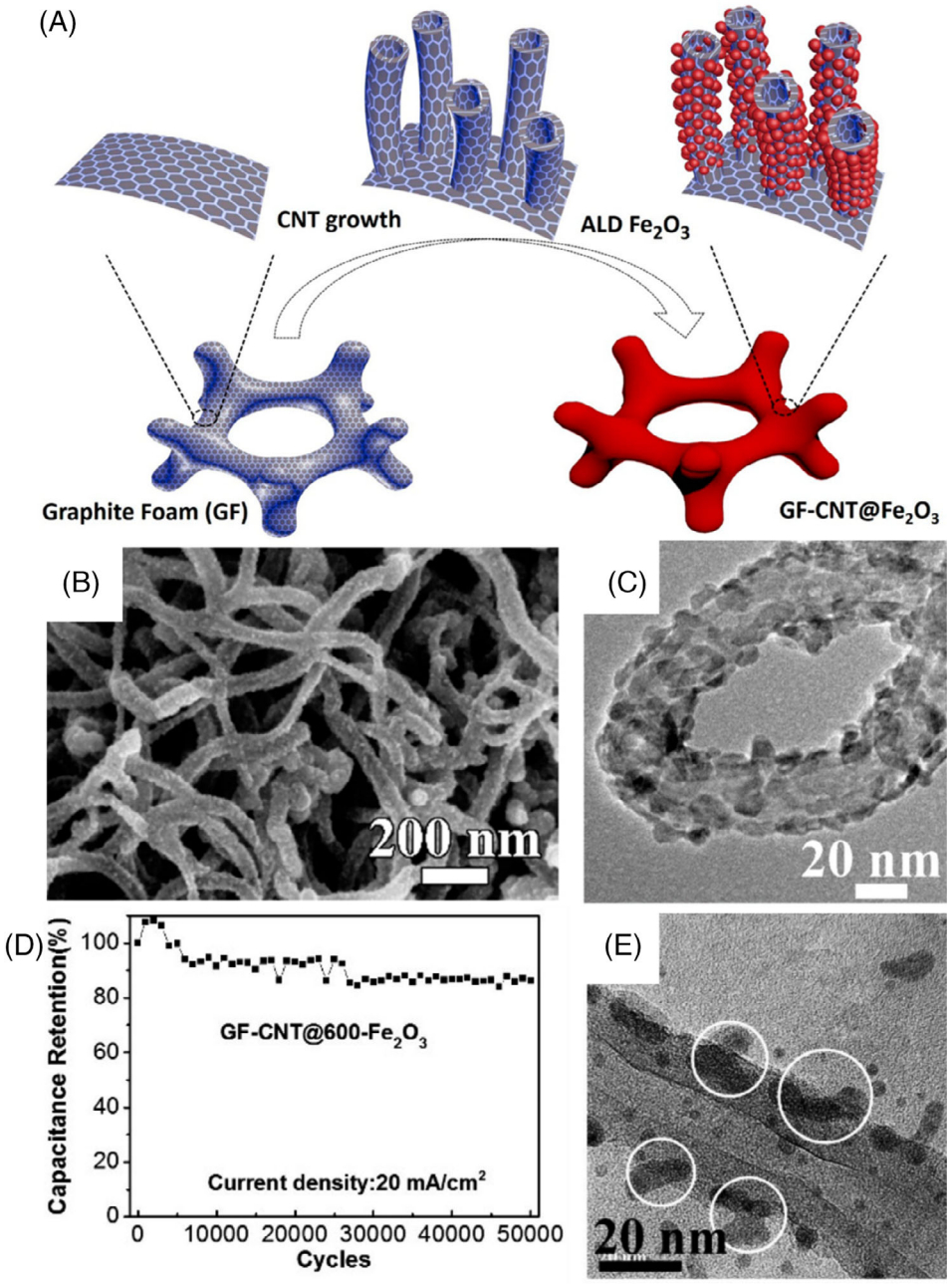

FIGURE 12 Graphite foam/CNT substrate stabilizes Fe_2O_3 nanoparticles. A, Scheme of the synthesis steps of GF-CNT@Fe_2O_3. B, Scanning electron microscopy (SEM) and, C, transmission electron microscopy (TEM) images of GF-CNT@Fe_2O_3. D, Cycling stability of GF-CNT@600-Fe_2O_3 in 2 M aqueous KOH electrolytes. E, TEM image showing the morphology of GF-CNT@600-Fe_2O_3 after cycling. The white circles highlight aggregated nanoparticles. Reproduced with permission from Reference 120. Copyright 2015, The American Chemical Society

CC/$NiCo_2O_4$-S (Figure 13B). After being deposited with NiO nanosheets, hierarchically structured CC/$NiCo_2O_4$-N@NiO and CC/$NiCo_2O_4$-S@NiO showed no capacitance loss after 12 000 charge-discharge cycles at 8 mA cm^{-2}. This outstanding stability was attributed to four factors: (a) the high mechanical strength of the entire electrodes; (b) the reduced charge-transfer resistance resulted from the nanocrystalline $NiCo_2O_4$ and NiO; (c) the inter-voids among nanosheets and nanoneedles (or nano-slices) buffering the mechanical strain; and (d) the enhanced electrical conductivity of $NiCo_2O_4$ compared to NiO lowering internal resistance. Importantly, verified by the SEM images collected before and after the stability test, the hierarchical structures of CC/$NiCo_2O_4$-N@NiO (Figure 13C,D) and CC/$NiCo_2O_4$-S@NiO (Figure 13E,F) both remained intact.

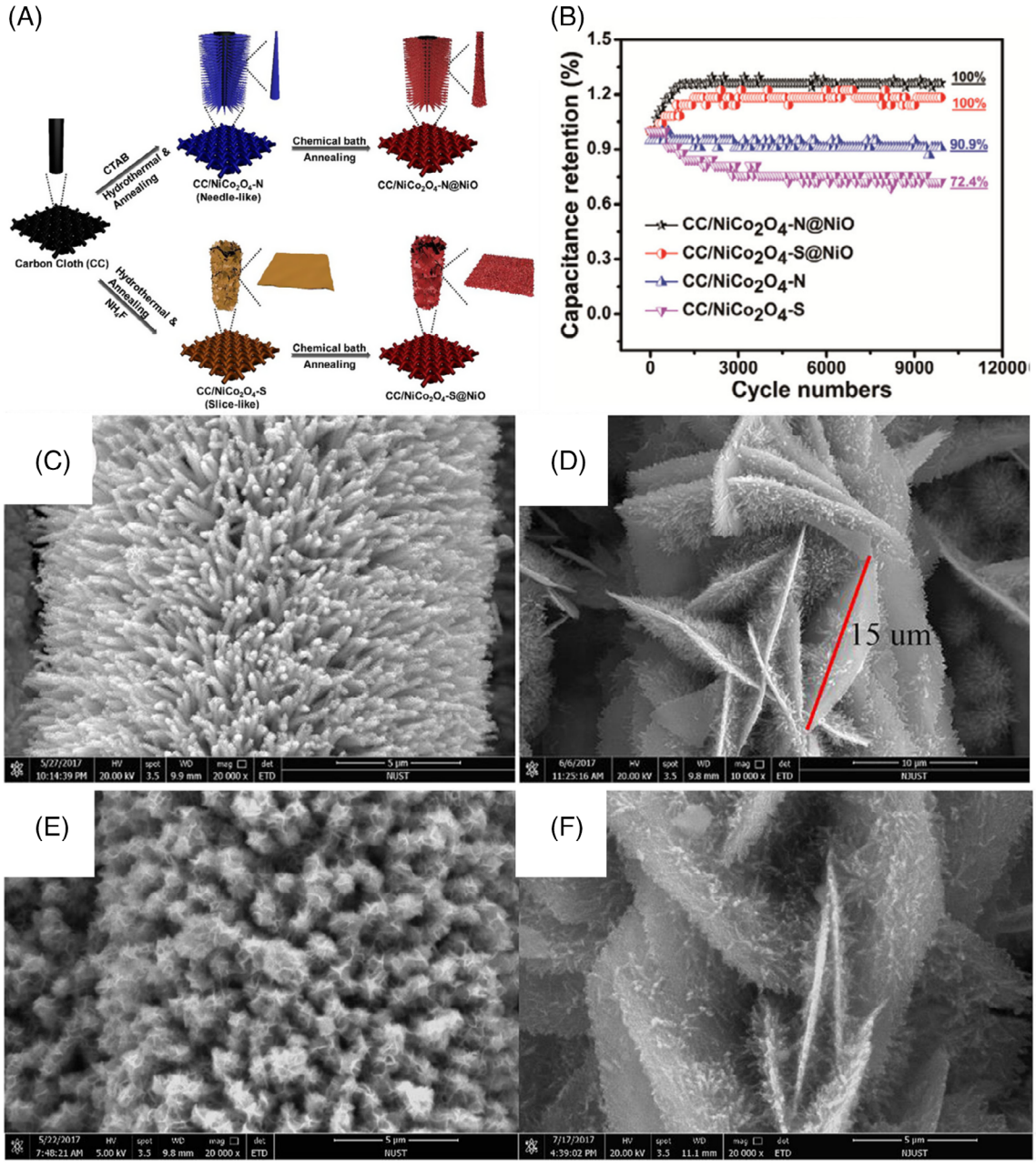

FIGURE 13 Hierarchical $NiCo_2O_4$/NiO nanostructures with enhanced cycling stability. A, Scheme of the syntheses of CC/$NiCo_2O_4$-N@NiO and CC/$NiCo_2O_4$-S@NiO. B, Cycling stability of various electrodes in 6 M aqueous KOH electrolytes. C-F, Scanning electron microscopy (SEM) images of electrodes before cycling: C, CC/$NiCo_2O_4$-N@NiO, D, CC/$NiCo_2O_4$-S@NiO, and after cycling: E, CC/$NiCo_2O_4$-N@NiO, F, CC/$NiCo_2O_4$-S@NiO. Reproduced with permission from Reference 144. Copyright 2019, Elsevier

3.2.3 | Gel electrolytes

Polymer-based gel electrolytes offer twofolded protections to metal oxides that liquid electrolytes cannot: Their elasticity and softness curtail the structural instability of metal oxides, and the low water content of gel electrolytes limits dissolution of water-soluble metal ions.[34] Poly(vinyl alcohol) (PVA)[62] and poly(methyl methacrylate) (PMMA)[33] are common polymers used to prepare gel electrolytes.

Penner and coworkers achieved extraordinary cycling stability of MnO_2 nanowires in PMMA gel electrolytes (Figure 14).[33] Using photolithography and electrodeposition, the researchers made interdigitate gold nanowires coated with δ-MnO_2 nanosheets (Au@MnO_2) (Figure 14A-C). PMMA gel electrolytes composed of 20 wt% PMMA and 1.0 M $LiClO_4$ in propylene carbonate were coated onto Au@MnO_2 nanowire arrays. Au@MnO_2 with different MnO_2 thicknesses showed consistently better cycling stability in the PMMA gel

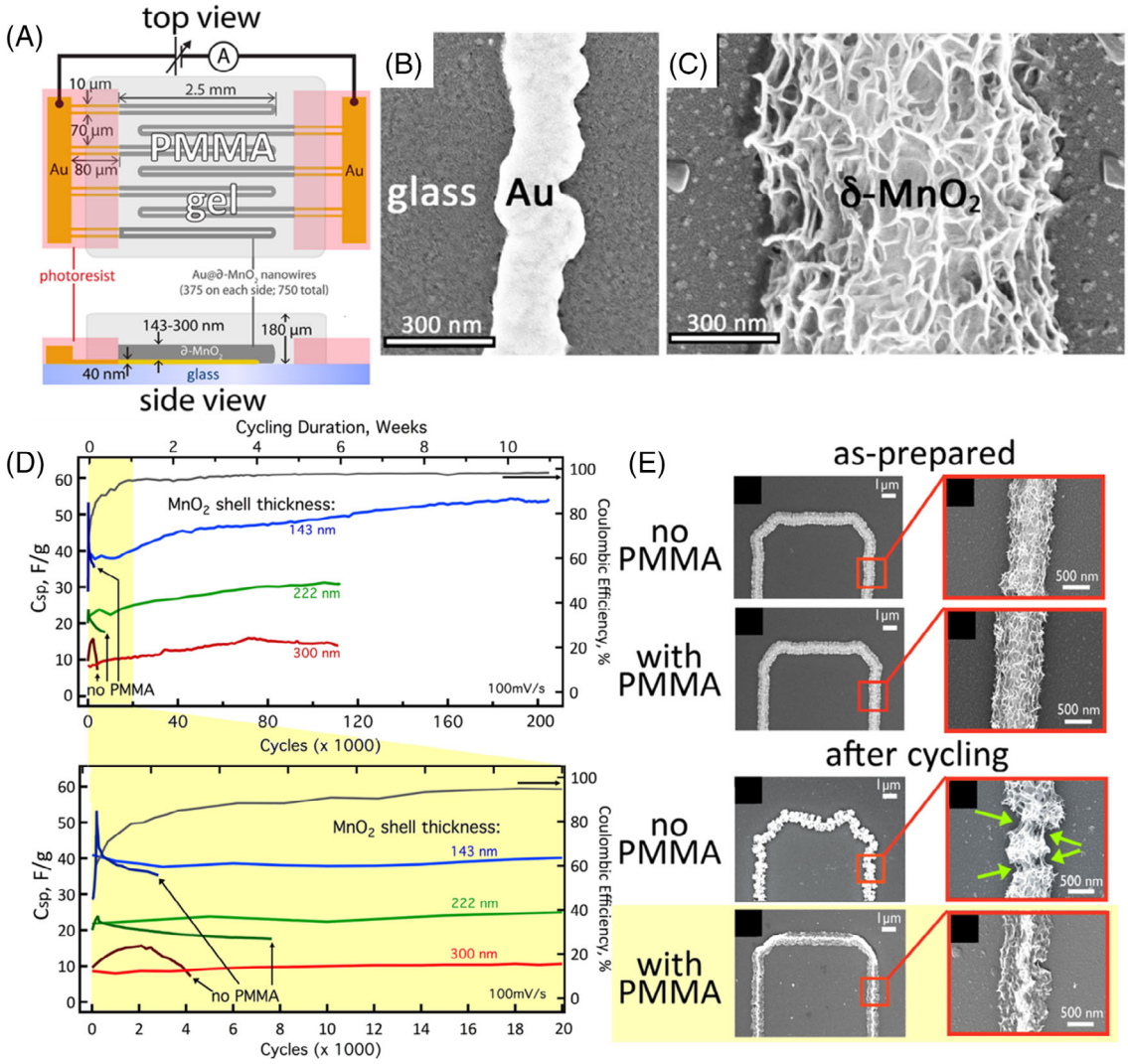

FIGURE 14 Poly(methyl methacrylate) (PMMA)/acetonitrile gel electrolytes stabilize δ-MnO_2 nanosheets. A, Scheme showing the dimensions of the interdigitated δ-MnO_2/Au electrodes. B,C, Scanning electron microscopy (SEM) images of, B, a bare Au nanowire and, C, a δ-MnO_2/Au nanowire. D, Cycling stability and, E, SEM images of δ-MnO_2/Au electrodes of different MnO_2 shell thicknesses in 1 M $LiClO_4$ acetonitrile electrolytes with and without PMMA. The green arrows point to crack sites. Reproduced with permission from Reference 33. Copyright 2016, The American Chemical Society

electrolytes than in propylene carbonate liquid electrolytes (Figure 14D). Au@MnO_2 nanowires with 143-nm-thick MnO_2 shells achieved the best cycling stability, experiencing no capacitance loss after 200 000 charge-discharge cycles. Post-mortem analysis using SEM revealed that the MnO_2 shells in the liquid electrolytes partially detached due to structure breakdown, whereas the MnO_2 shells were well preserved in the PMMA gel electrolytes. These results signified that gel electrolytes prevented the dissolution of δ-MnO_2 (Figure 14E).

Wang et al demonstrated that PVA/LiCl gel electrolytes effectively suppressed the dissolution of vanadium oxide nanowires.[62] The unsatisfactory cycling stability of vanadium oxide in aqueous electrolytes mainly results from the formation of water-soluble vanadium species during charge and discharge (Section 2.3). Substituting aqueous electrolytes with gel electrolytes reduces water contents but still retains the ion diffusion capability of electrolytes, thus minimizing vanadium oxide dissolution. Experimental results showed that vanadium oxide nanowires in the PVA/LiCl gel electrolyte displayed approximately nine times higher capacitance retention than those in a 5 M LiCl aqueous electrolyte over 5000 charge-discharge cycles (Figure 15A). Compared to the vanadium oxide nanowires before cycling (Figure 15B), nanowires cycled in aqueous electrolytes almost disappeared (dissolution) and cracked (volumetric expansion) (Figure 15C), while those covered with gel electrolytes were preserved and visible under SEM (Figure 15D).

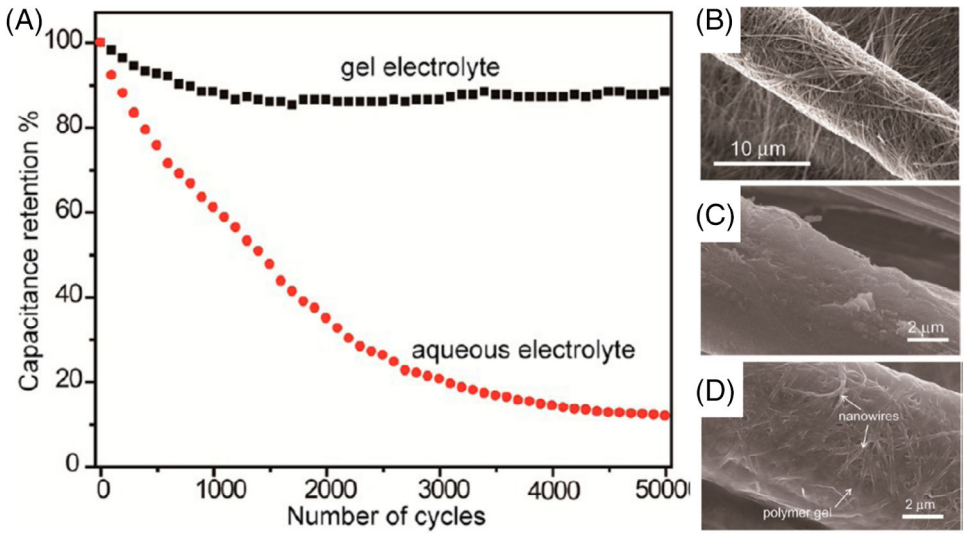

FIGURE 15 Poly(vinyl alcohol) (PVA)/LiCl gel electrolytes stabilize vanadium oxide nanowires. A, Cycling stability of vanadium oxide nanowires in 5 M aqueous LiCl electrolytes and LiCl/PVA gel electrolytes. B-D, Scanning electron microscopy (SEM) images of vanadium oxide nanowires on commercial carbon fibers: B, before and, C, after cycling in aqueous LiCl electrolytes and, D, gel LiCl electrolytes. Reproduced with permission from Reference 62. Copyright 2012, The American Chemical Society

3.2.4 | Valence state engineering

Tuning valence states of metal oxides directly curbs dissolution. This method requires comprehension of the interplays among valence state, electrical conductivity, thermodynamic stability, and electrochemical activities. Typically, increasing the concentrations of active and stable valence states in metal oxides promotes long-lasting performance. Reported valence-tuning methods include electrooxidation,[149] electroreduction,[119] elemental doping,[150] building oxide-based heterostructures,[151] and changing potential window.[48] Despite its versatility, valence tuning must be meticulously performed to avoid stability enhancement at the cost of capacitance.

Song et al demonstrated an example of stabilizing amorphous vanadium oxide nanowires by electrically reducing some V^{5+} to V^{4+} in vanadium oxide.[119] The rationale of introducing low valent vanadium species was that VO_2 is thermodynamically stable and water-insoluble at negative potentials in neutral aqueous electrolytes.[152] Vanadium oxide nanowires were first deposited via CV on electrochemically exfoliated carbon fibers, followed by electroreduction at −1.5 V (vs saturated calomel electrode) for 1 minute in 0.1 M vanadyl sulfate and 0.2 M ammonium acetate aqueous solutions at room temperature. This process shifted the V^{4+}/V^{5+} ratio from ~40% to ~50%. Cycling test showed that the reduced vanadium oxide on exfoliated carbon fiber (ECC/RVO_x) exhibited the best stability performance, exhibiting no capacitance loss after 100 000 charge-discharge cycles at 60 mA cm^{-2} (Figure 16A). In contrast, the as-deposited vanadium oxide on exfoliated carbon fibers (ECC/VO_x) experienced constant capacitance degradation starting from the beginning of the cycling test, and only maintained ~70% capacitance after 10 000 cycles. The initial capacitance loss of reduced vanadium oxide on the untreated carbon fibers (CC/RVO_x) was due to the structural collapse of RVO_x, and it steadily raised back to ~80% retention after 20 000 cycles. SEM images of the cycled electrodes revealed that the structure of ECC/RVO_x was well preserved (Figure 16B), but the nanowires of ECC/VO_x and CC/RVO_x dissolved (Figure 16C) and detached (Figure 16D), respectively. The discrepancy in cycling stability highlighted two advantages of ECC/RVO_x: The exfoliated carbon shells of ECC avoided the volumetric-deformation-induced structural collapse of vanadium oxide, and the increased concentration of V^{4+} suppressed nanowire dissolution. Additionally, XPS elucidated that V^{4+}/V^{5+} ratios of the three electrodes all increased during the cycling, and that of ECC/VO_x plateaued at ~60% (Figure 16E). The observation suggested that the valence state of V underwent a dynamic transition that enriched tetravalence. Additionally, O 1s XPS spectrum of ECC/RVO_x showed that the peak intensities of structural water and V—OH gradually increased (Figure 16F). The continuous hydration of vanadium oxide was possibly a result of water uptake during the activation process at the beginning of the stability test. Nyquist plots unveiled that the water incorporation facilitated ion diffusion within the reduced vanadium oxide nanowires, as evident from

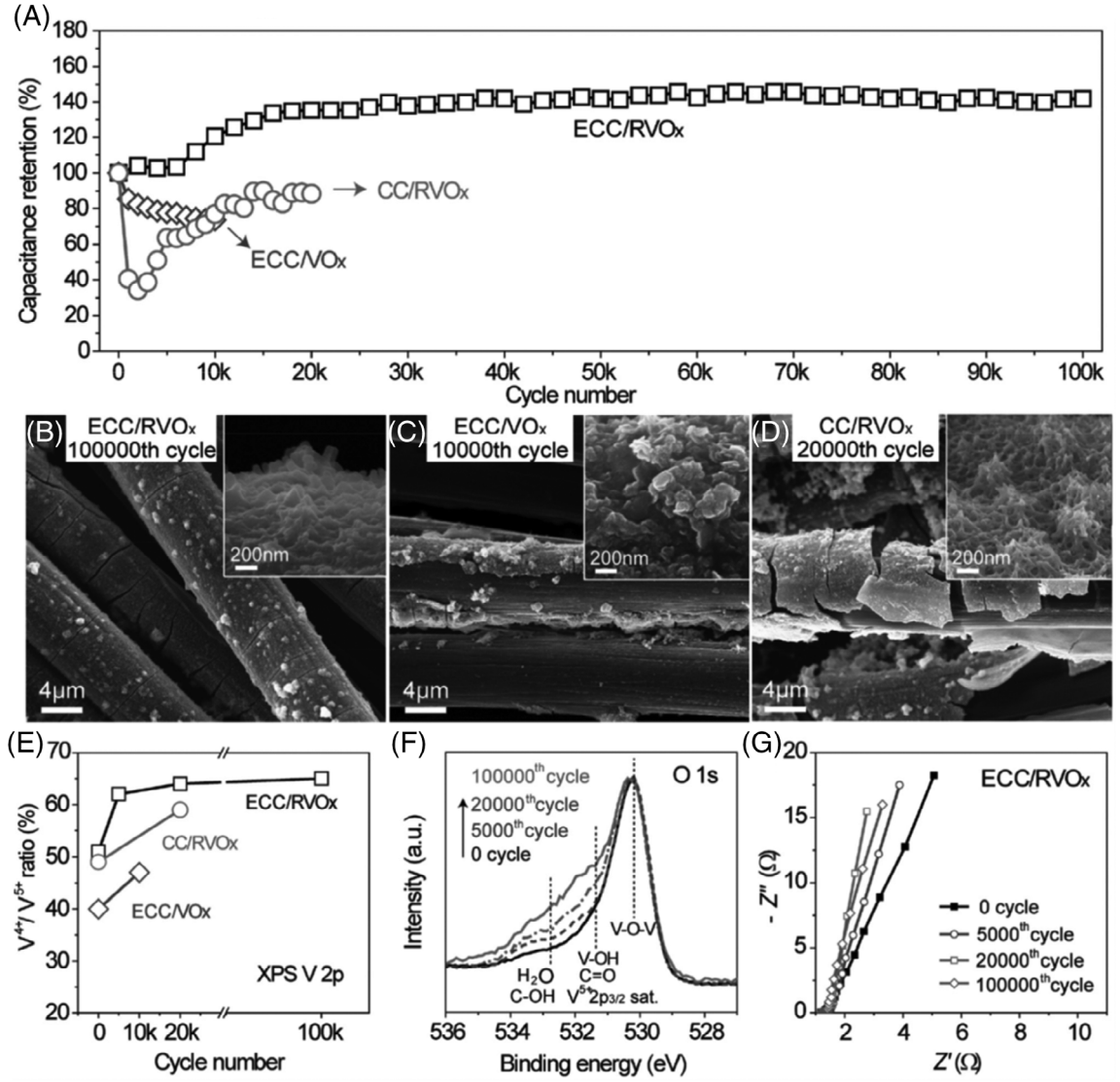

FIGURE 16 Varying valence states stabilizes vanadium oxide nanowires. A, Cycling stability of ECC/RVO_x, ECC/VO_x, and CC/RVO_x in 5 M aqueous LiCl electrolytes. B-D, Scanning electron microscopy (SEM) images of, B, ECC/RVO_x, C, ECC/VO_x, and, D, CC/RVO_x after 100 000 consecutive charge–discharge cycles. E, V^{4+}/V^{5+} ratios of the three electrodes at different cycle numbers. F, O 1s XPS spectra and, G, Nyquist plots of ECC/RVO_x at different cycle numbers. Reproduced with permission from Reference 119. Copyright 2017, WILEY-VCH Verlag GmbH & Co

the increasing slope of the diffusion tails in the low-frequency domain (Figure 16G).

3.2.5 | Ion preinsertion

Inserting immobile guest ions is a potent structure-stabilization method for metal oxides possessing tunneled or layered structures. The intentionally introduced ions need to bind strongly with the channel walls or layers of the host metal oxides, which prevents these ions from leaking out at high potentials. The inserted ions, therefore, function as structure scaffolds to minimize the structure expansion of metal oxides and impede pulverization. It is noteworthy that the effectiveness of this strategy is material dependent. One needs to consider the compatibility of the guest ions with their hosts. For example, Yao et al observed that introducing hydrated zinc and gallium ions in between δ-MnO_2 layers stabilized capacitance (no capacitance loss after 20 000 charge-discharge cycles), but Fe^{3+}-intercalated δ-MnO_2 showed rapid capacitance decay (~10% capacitance retention) under identical testing conditions.[36] The discrepancy in the cycling stability performance was attributed to the different interaction strength between the cations and the δ-MnO_2 layers.

3.3 | Metal nitrides and carbides

3.3.1 | Protective encapsulation

Encapsulation provides metal nitrides and carbides physical barriers to prevent their contact with oxidants (eg, water and oxygen gas) and, thus, to halt oxidation. Most coating materials are electrically conductive to maintain the high electrical conductivity of the entire materials. Demonstrated coatings are composed of amorphous carbon shells derived from glucose,[41] polydopamine,[153] poly (acrylonitrile),[154] polymeric nano-micelles,[155] rGO,[156-159] and conjugated polymers.[160-162] Occasionally, ultrathin metal oxide layers are used to stabilize metal nitrides,[163] but the main purpose is to facilitate electron flow into the metal oxide coatings from the coated metal nitrides. The thickness of coatings is a critical parameter that needs optimization to avoid compromising the capacitance and rate capability of the encapsulated materials: Too thin coatings might be incomplete and provide limited protection; too-thick coverage could block ion accessibility into the coated materials and reduce capacitance. In situ or *operando* characterizations are valuable in acquiring fundamental understandings on the ion diffusion mechanisms across coatings, which is currently scarce but will aid the rational design of the thickness, porosity, and composition of the coating materials.

To mitigate the oxidation problem of TiN, Lu et al developed a carbon-coating method.[41] The carbon layers were first produced by decomposing glucose in a hydrothermal reaction, followed by thermal annealing at 800°C under N_2 atmosphere (Figure 17A) to convert the glucose-decomposed products into carbon. The lattice-resolved TEM image (Figure 17B) showed that a 1.5-nm-thick, amorphous carbon layer was uniformly deposited on a single-crystalline TiN nanowire (TiN@C). This carbon layer substantially elevated the capacitance retention of the TiN nanowires to ~92% after 15 000 charge-discharge cycles in 1 M aqueous KOH electrolytes (Figure 17C). In sharp contrast, the uncoated TiN nanowires retained only ~9% capacitance under the same testing conditions. SEM (Figure 17D) and XPS (Figure 17E) of the cycled TiN@C nanowires proved that the structure and surface functionalities remained unchanged, respectively.

3.3.2 | Tuning electrolyte composition

As moisture is one of the culprits oxidizing the surfaces of metal nitrides and carbides, reducing water contents in electrolytes is beneficial to slow down or stop the oxidation of metal nitrides and carbides. Therefore, gel electrolytes (mainly PVA-based)[42,159,164] and organic electrolytes[165] with little or no water could stabilize metal nitrides and carbides. Recently, researchers have discovered that neutral electrolytes also prolong the lifetimes of metal nitride electrodes, owing to an equilibrium between dissolved metal ions and solid-state metal nitrides that decelerates surface oxidation.[166,167]

One representative PVA-based gel electrolyte that stabilized TiN nanowires was reported by Lu et al.[42] The researchers added PVA powder into KOH aqueous solutions to convert the liquid solutions into PVA/KOH gel electrolytes. These electrolyte thin films were then sandwiched between TiN nanowires grown on carbon cloth, followed by being hot-pressed to infiltrate the inter-wire space among the TiN nanowires (Figure 18A). As a result of surface oxidation, TiN nanowires cycled in aqueous KOH electrolytes showed apparent capacitance decay, with less than 10% capacitance remained after the first 3000 charge-discharge cycles. In contrast, TiN nanowires incorporated with PVA/KOH held 83% of its initial capacitance at the same cycle number (Figure 18B). TiN nanowires cycled in PVA/KOH also retained their morphology (Figure 18C) and only mildly oxidized, as evidenced by the slight reduction in the XPS peak area of Ti—N bond (Figure 18D).

3.3.3 | Cation intercalation

For metal nitrides and carbides with layered structures, for example, MXenes, guest species in between their layers could change their intrinsic electronic properties and improve their oxidation resistance. For example, VahidMohammadi et al reported that intercalating Li^+ or Na^+ into V_2CT_x (T_x stands for surface functional groups of —OH, —O, and —F), a layered metal carbide, could make it air-stable and electrochemically robust.[168] The researchers first dispersed V_2CT_x nanosheets in water and mixed with concentrated aqueous solutions of LiCl and NaCl. Since V_2CT_x nanosheets were negatively charged, these cations preferably adsorbed onto V_2CT_x nanosheets. After filtration and drying to stack the ion-adsorbed V_2CT_x nanosheets together, self-standing V_2CT_x films intercalated with Li^+ or Na^+ were prepared (Figure 19A). Outstandingly, in various aqueous electrolytes, Na^+-intercalated V_2CT_x films showed almost no loss of capacitance after cycling for 10 000 cycles in various aqueous electrolytes (Figure 19B), in sharp contrast to intercalant-free V_2CT_x films which lost more than 30% capacitance after merely 1500 cycles in 5 M aqueous LiCl electrolytes (Figure 19C). Additionally, the difference in the

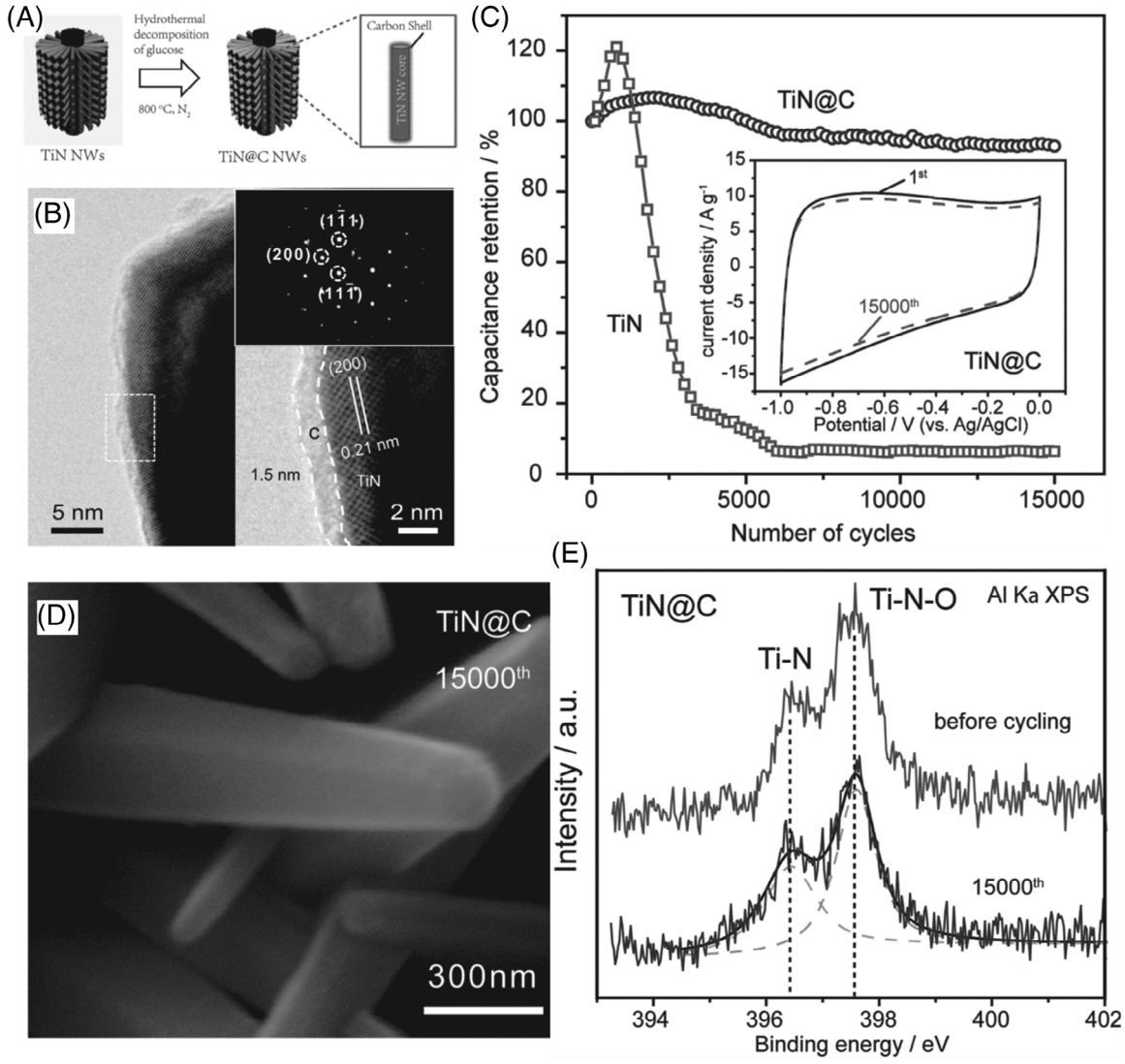

FIGURE 17 Carbon coating stabilizes TiN nanowires. A, Scheme of a glucose-assisted hydrothermal reaction to coat thin carbon shells onto TiN nanowires. B, Lattice-resolved transmission electron microscopy (TEM) image of TiN@C. C, Cycling stability of TiN and TiN@C in 1 M aqueous KOH electrolytes. D, Scanning electron microscopy (SEM) of TiN@C after cycling. E, Core-level N 1s XPS spectra of TiN@C before and after cycling. Reproduced with permission from Reference 41. Copyright 2014, WILEY-VCH Verlag GmbH & Co

film integrity between the cycled Li^+-intercalated V_2CT_x and intercalant-free V_2CT_x films corroborated the cycling performance (Figure 19D). Additionally, XPS showed that compared to as-prepared V_2CT_x (Figure 19E), intercalant-free V_2CT_x contained much more oxidation products V^{5+} after exposing to air in 1 month (Figure 19F); however, the concentrations of all V-cations in Li^+-intercalated, air-exposed V_2CT_x were comparable to those of as-prepared V_2CT_x (Figure 19G), suggesting no appreciable oxidation happened. Density functional theory further found that electrons could transfer from the intercalants to the surfaces of V_2CT_x and primarily reside near the —F surface groups. This electron redistribution made V_2CT_x more negatively charged and oxidation resistant.

3.4 | Metal sulfides

3.4.1 | Mechanical buffering

Similar to metal oxides, metal sulfides, especially those with layered structures that can host guest molecules between adjacent layers, suffer from capacitance loss due to structure breakdown. To remedy these problems, incorporation metal

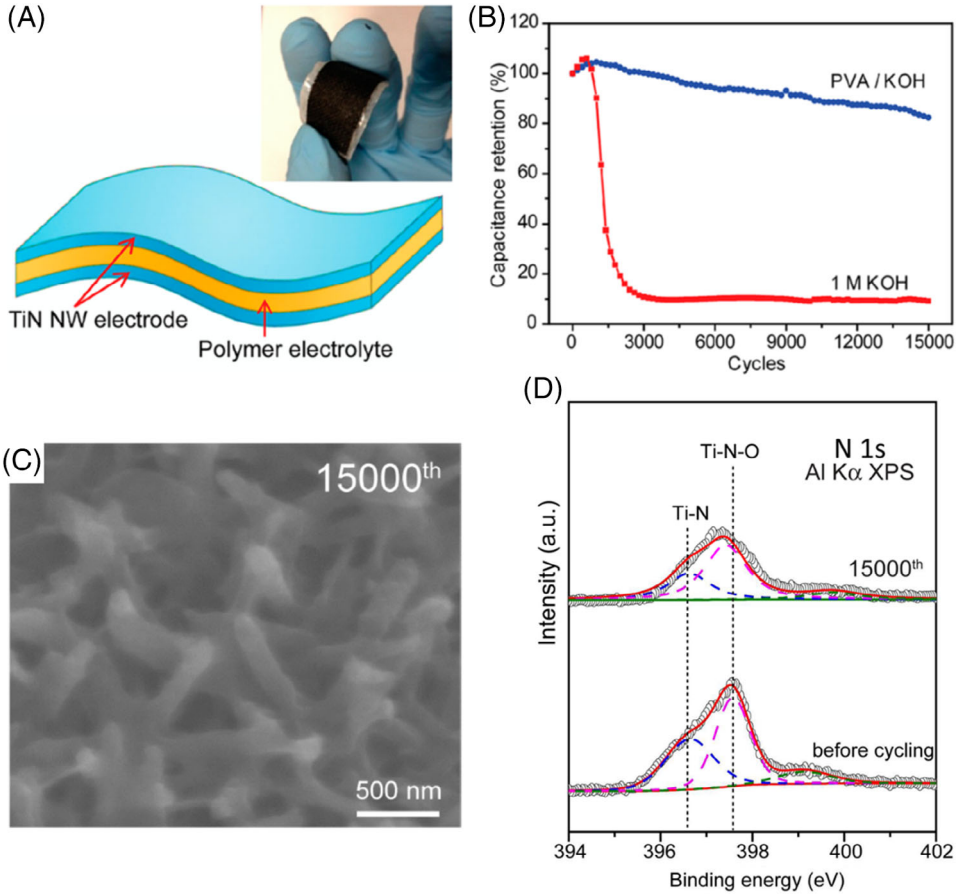

FIGURE 18 Poly(vinyl alcohol) (PVA)/KOH gel electrolytes stabilize TiN nanowires. A, Scheme of a pseudocapacitor with a PVA/KOH gel electrolyte. Inset: flexibility of the pseudocapacitor. B, Cycling stability of TiN nanowires in a 1 M aqueous KOH electrolyte and a PVA/KOH gel electrolyte. C, Scanning electron microscopy (SEM) image of TiN nanowires after 15 000 consecutive charge–discharge cycles in PVA/KOH. D, Core-level N 1s XPS spectra of TiN nanowires before and after cycling in PVA/KOH. Reproduced with permission from Reference 42. Copyright 2012, The American Chemical Society

sulfides with flexible substrates or wrappings become a popular strategy. Carbon materials, including carbon dots,[169] graphene or rGO,[170-176] carbon nanotubes,[177-180] carbon coatings,[177,181,182] and three-dimensional carbon foams or aerogels,[183-186] are the most adopted materials because of their structural flexibility and high electrical conductivity. Structurally stable metal oxides (eg, NiO,[187]) or amorphous metal sulfides (eg, amorphous Co_3S_4[188]) are occasionally selected to stabilize metal sulfides. Besides functioning as mechanical buffers, these substrates and wrappings could also anchor metal sulfide nanoparticles and prevent the small particles from coalescing during charge and discharge, promoting long lifetimes.

Lee, Kim, and coworkers demonstrated one excellent example of graphene wrapping to stabilize metal sulfides.[170] Specifically, the authors covered Co_8FeS_8 and FeS nanoparticles with nitrogen-doped graphene (NG) sheets via a hydrothermal reaction (Figure 20A). High-resolution TEM image presented that Co_8FeS_8 nanoparticles were uniformly covered with graphene sheets without severe local aggregation (Figure 20B). The mechanical robustness and high cycling stability of the N-doped graphene nearly doubled the cycling stability of Co_8FeS_8, compared to that of bare Co_8FeS_8, after 10 000 charge-discharge cycles in 2 M aqueous KOH electrolytes (Figure 20C). SEM images of the cycled nitrogen-graphene wrapped Co_8FeS_8 (Co_8FeS_8@NG) showed no particle degradation or aggregation before and after cycling (Figure 20D,E), proving that NG wrapping was beneficial to stabilize and prevent nanoparticle aggregation.

3.4.2 | Structure engineering

Besides wrapping or supporting metal sulfides with flexible materials, nanostructured metal sulfides showed improved structural integrity. The rationale of this strategy is to accommodate the volumetric deformation of metal sulfides using the empty spaces among nanostructures. To date, a plethora of nanostructured metal sulfides, including hollow particles,[179,189,190] nanosheets/nanoplates,[191-195]

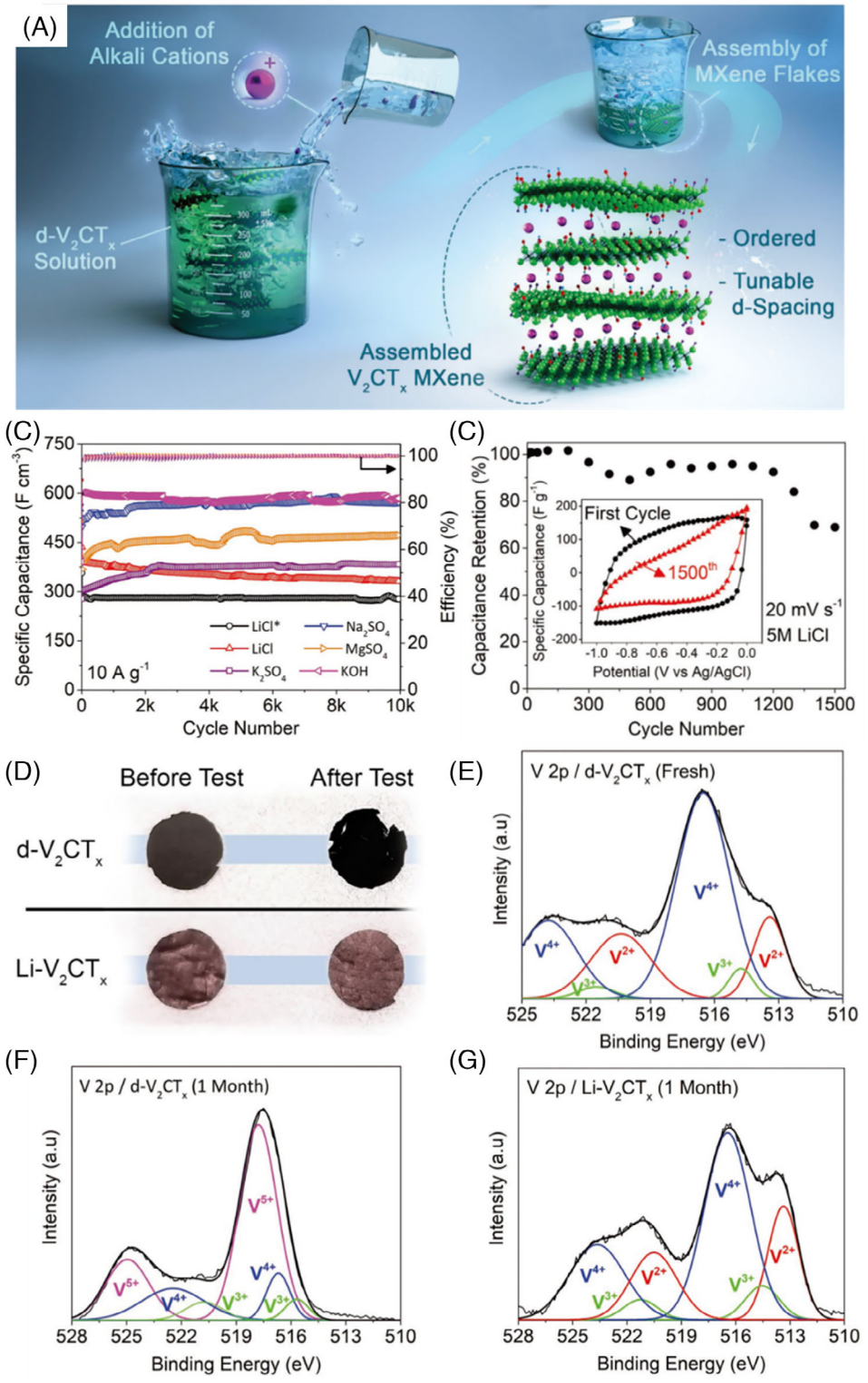

FIGURE 19 Cation intercalation stabilizes V_2CT_x nanosheets. A, Scheme of intercalating cations into V_2CT_x nanosheets. B, Cycling stability performance of Na^+-intercalated V_2CT_x in various aqueous electrolytes. LiCl* represents Li^+-intercalated V_2CT_x tested in a 5 M LiCl aqueous electrolyte. C, Cycling instability of pristine V_2CT_x in a 5 M LiCl aqueous electrolyte. D, Oxidation stability of pristine V_2CT_x and Li^+-intercalated V_2CT_x films. E-G, V 2p XPS spectra of, E, as-prepared V_2CT_x, F, intercalant-free V_2CT_x placed in air for 1 month, and, G, Li^+-intercalated V_2CT_x placed in air for 1 month. Reproduced with permission from Reference 168. Copyright 2019, WILEY-VCH Verlag GmbH & Co

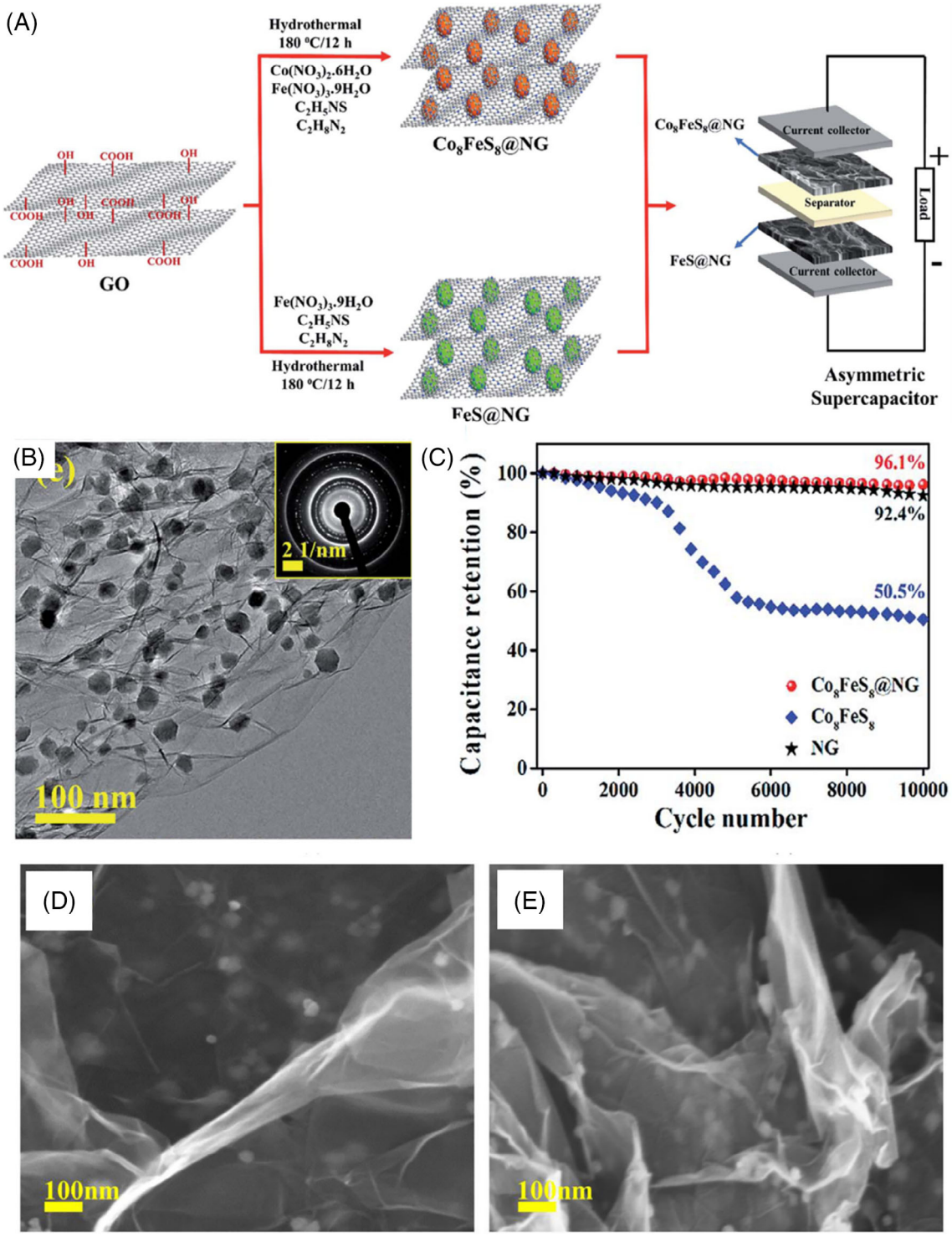

FIGURE 20 N-doped graphene (NG) wrapping stabilizes Co_8FeS_8 nanoparticles. A, Scheme of the synthesis steps of Co_8FeS_8@NG and FeS@NG. B, Low-magnified transmission electron microscopy (TEM) image of Co_8FeS_8@NG showing the uniform distribution of Co_8FeS_8 nanoparticles. Inset: selected area electron diffraction pattern of the imaged region. C, Cycling stability of Co_8FeS_8@NG, Co_8FeS_8, and NG in 2 M aqueous KOH electrolytes. D,E, Scanning electron microscopy (SEM) images of Co_8FeS_8@NG, D, before and, E, after 10 000 charge–discharge cycles. Reproduced with permission from Reference 170. Copyright 2019, The Royal Society of Chemistry

nanoflowers,[196-199] nanowires,[200] nanotubes,[201] and hierarchical architectures integrating multiple nanostructures have displayed improved cycling stability.[202,203]

Huang et al reported a hierarchical structure involving nanotubes and nanosheets for stabilizing Co_9S_8.[203] They first grew ZnO nanowires onto commercial carbon

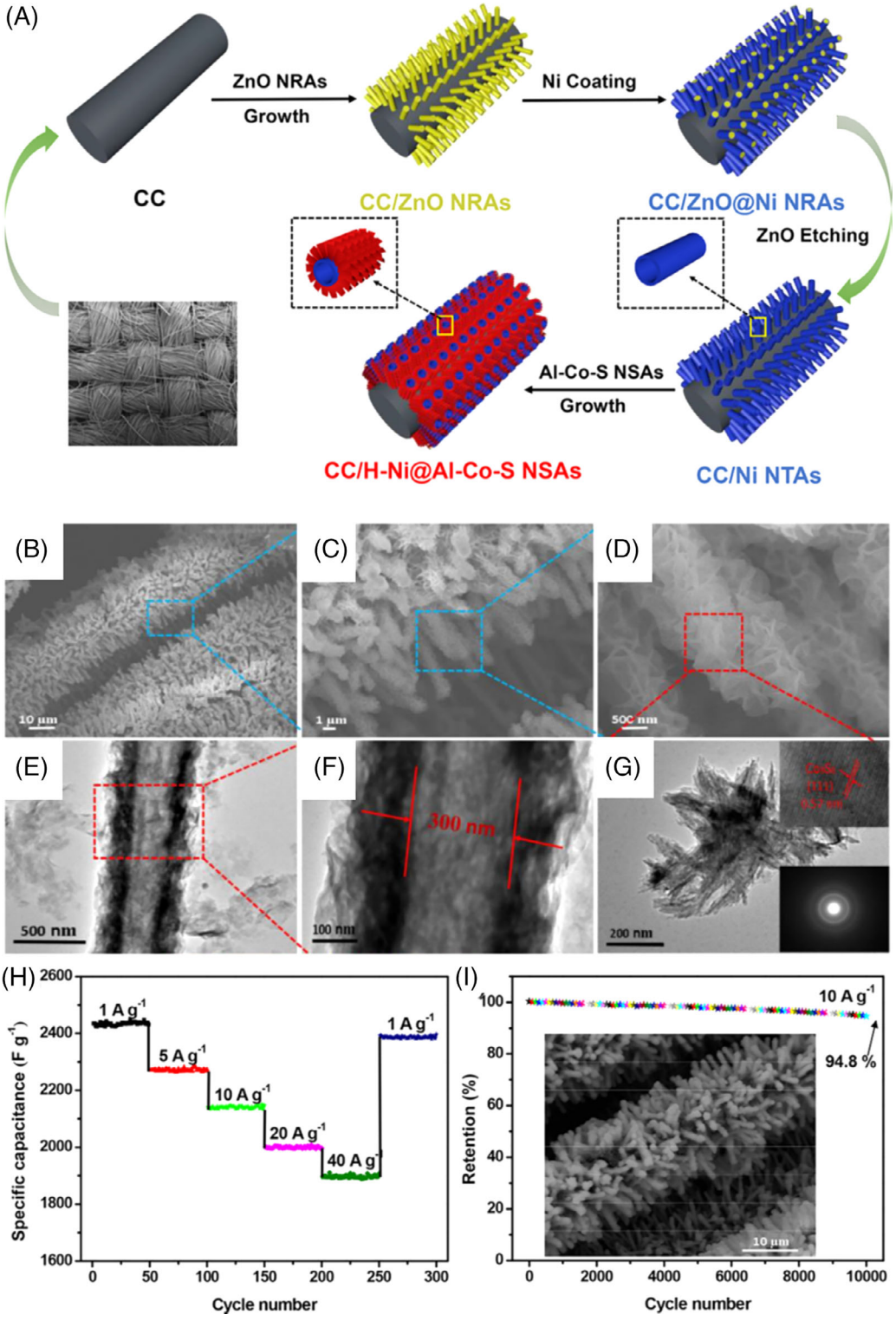

FIGURE 21 Al-doped Co_9S_8 nanosheets on Ni nanotube arrays supported on carbon fibers (CC/H-Ni@Al-Co-S NSAs) nanosheets exhibit excellent cycling stability. A, Scheme of the synthesis steps of CC/H-Ni@Al-Co-S NSAs. B-D, Scanning electron microscopy (SEM) and transmission electron microscopy (TEM), E-G, images of CC/H-Ni@Al-Co-S NSAs at different magnifications. H, Rate capability and, I, cycling stability of CC/H-Ni@Al-Co-S NSAs in 2 M aqueous KOH electrolytes. Inset: SEM image of CC/H-Ni@Al-Co-S NSAs after cycling. Doping Al improved the electrical conductivity of Co_9S_8. CC, carbon cloth; NRA, nanorod array; NTA, nanotube array. Reproduced with permission from Reference 203. Copyright 2018, The American Chemical Society

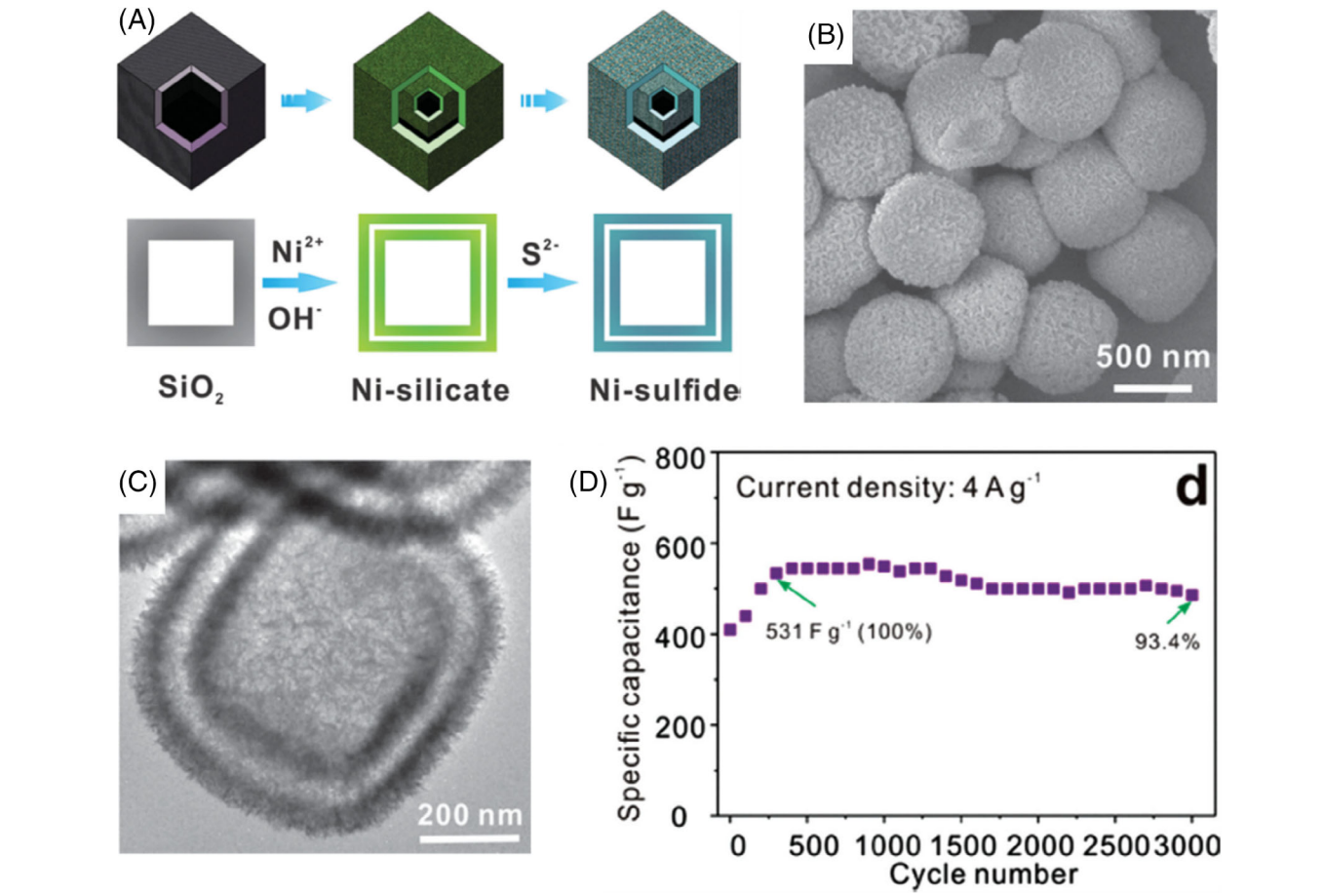

FIGURE 22 Box-in-box NiS nanoparticles with stable electrochemical performance. A, Scheme of the morphology and composition evolutions during the synthesis of box-in-box NiS nanoparticles. B, Scanning electron microscopy (SEM) and, C, transmission electron microscopy (TEM) images of a box-in-box NiS nanoparticle. D, Cycling stability of box-in-box NiS nanoparticles in a 3 M KOH aqueous electrolyte. Reproduced with permission from Reference 189. Copyright 2014, WILEY-VCH Verlag GmbH & Co

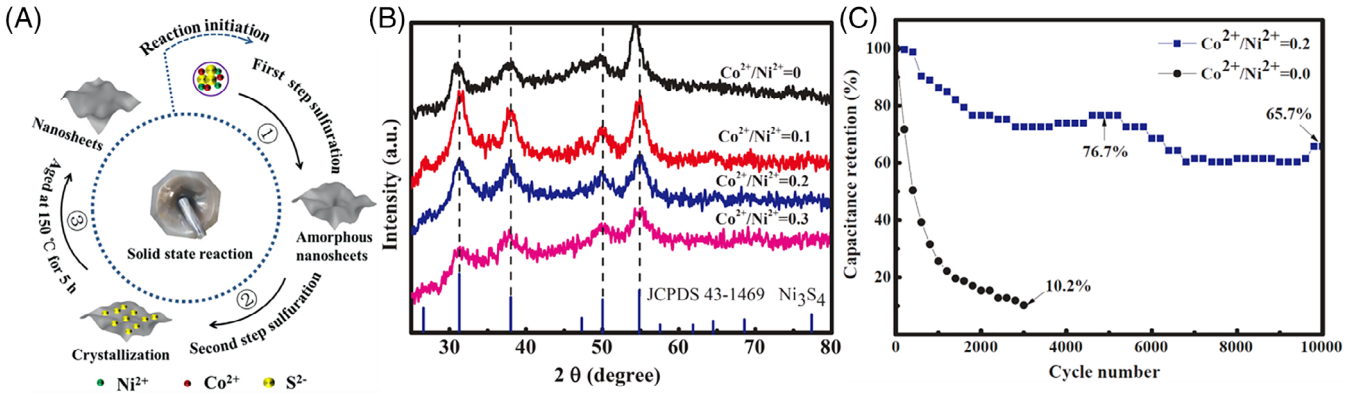

FIGURE 23 Co^{2+}-doping stabilizes Ni_3S_4 nanosheets. A, Scheme of the synthesis steps toward Co^{2+}-doped Ni_3S_4. B, XRD diffraction patterns of Ni_3S_4 with different concentrations of Co^{2+} dopants. C, Cycling stability of Ni_3S_4 nanosheets with and without Co^{2+} dopants in 3 M aqueous KOH electrolytes. The gradual increase in capacitance retention between 3000th and 5000th cycles of Co^{2+}-doped Ni_3S_4 was due to temperature change. Reproduced with permission from Reference 206. Copyright 2019, Elsevier

fibers, plated with Ni metal, and dissolved ZnO to obtain Ni nanotube arrays on carbon fibers. These metallic arrays were then electrodeposited with Co_9S_8 nanosheets (Figure 21A). SEM images demonstrated that Ni/Co_9S_8 nanotubes grew uniformly on each carbon fiber, and Co_9S_8 nanosheets covered the Ni

nanotubes conformally (Figure 21B-D). TEM images illustrated the hollow tubes and the coated polycrystalline Co_9S_8 nanosheets (Figure 21E-G). This hierarchical architecture not only facilitated ion diffusion to render excellent rate capability (Figure 21H) but also effectively suppressed the structure disintegration of Co_9S_8 to bestow the high cycling stability in 2 M aqueous KOH electrolytes (Figure 21I). The hierarchical structure remained intact after cycling (Figure 21I inset).

Lou and coworkers reported a general strategy of synthesizing box-in-box shaped metal sulfide nanoparticles with excellent cycling performance.[189] They first synthesized SiO_2 nano-boxes using Fe_2O_3 nanocubes as sacrificial templates, followed by dispersing these SiO_2 nano-boxes into aqueous solutions containing nickel acetate, ammonia, and ammonia chloride. The weak alkaline environment provided by the buffer system of ammonia and ammonia chloride slowly dissolved SiO_2 into silicate anions, which reacted with Ni^{2+} and formed nickel silicate. The diffusion-limited kinetics of Ni^{2+} resulted in the double-walled nickel silicate hollow cubes (Figure 22). Afterward, the double-walled nickel silicate particles were converted to nickel sulfide by sulfurization. The synthesized NiS double-walled boxes were coated with dense and uniform nanosheets both on the outer and inner surfaces of the boxes (Figure 22B,C). Having the unique box-in-box configuration that alleviated the destruction power of volumetric swelling and shrinkage, the double-walled, hollow NiS particles retained 93.4% capacitance after 3000 charge-discharge cycles at 4 A g^{-1} (Figure 22D). In comparison, the capacitance of solid NiS particles continually decreased during 1500 charge-discharge cycles at 4 A g^{-1}.

3.4.3 | Doping

Doping has dual effects in enhancing the cycling stability of metal sulfides. It reduces electrical resistance to minimize joule heating, as well as tunes crystal structures to metal sulfides with inherently good cycling stability. Inspired by previous experimental observations that Co_3S_4 showed superior cycling stability,[204,205] Li et al, conceived the idea of doping Co^{2+} to stabilize Ni_3S_4 nanosheets.[206] The doping was realized by a solid-state reaction where precursors of Ni_3S_4 along with cobalt nitrate hexahydrate (the Co^{2+} source) were ground and mixed thoroughly, followed by aging at 150°C for 5 hours (Figure 23A). XRD showed that all the diffraction peaks of Ni_3S_4 consistently shifted to slightly larger diffraction angels (Figure 23B), indicating the successful doping of Co^{2+}. Since the crystallographic structure of Co_3S_4 is identical to that of Ni_3S_4, there were no new XRD peaks after Co^{2+}-doping. Co^{2+}-doped Ni_3S_4 and pristine Ni_3S_4 have quite different cycling stability: The former kept 65.7% of its initial capacitance after 10 000 cycles, while the latter's capacitance dropped to 10.2% after only 2500 cycles (Figure 23C). The stability enhancement was attributed to the partial conversion of Ni_3S_4 to Co_3S_4 with inherently better cycling stability.

4 | SUMMARY AND OUTLOOK

This review has described the typical failure modes and possible resolutions of five most commonly used pseudocapacitive materials: conjugated polymers, metal oxides, metal nitrides, metal carbides, and metal sulfides. This information, along with selected examples, is summarized in Table 1.

Cycling stability, as a crucial performance metric for pseudocapacitive materials, will continue to be extensively characterized for emerging electrode materials. Herein we would like to highlight four issues associated with cycling stability that could serve as useful guidelines for future researches.

First, researchers must avoid confusions between battery-like materials and pseudocapacitive materials. Pseudocapacitive materials store charges via Faradic redox reactions with fast kinetics. Their electrochemical signatures are similar to traditional electrical double layer capacitive materials (eg, activated carbon): rectangular-shaped cyclic voltammograms and sloping potential-time GCD profiles (Figure 24A,B). A pseudocapacitive material could show some deviations but should behave similarly to electrical double layer capacitive materials (Figure 24C, D). Differently, battery-like materials that undergo diffusion-controlled reactions often have sluggish kinetics, and their cyclic voltammograms contain sharp, well-defined peaks whose peak potentials are nonoverlapping (Figure 24E). Correspondingly, GCD profiles of battery-like materials have clear plateaus at different voltages in both charging and discharging (Figure 24F). Protocols on the performance evaluation, result interpretation, and data presentation between pseudocapacitive and battery-like materials are drastically different. This information, as well as nontypical cases of pseudocapacitive processes and detailed differentiation criteria, are available in several excellent articles.[68,207,208] Thoroughly discussing the details are beyond the scope of this review, but we strongly encourage researchers, particularly new practitioners in electrochemical energy storage, to read these papers. Correctly identifying pseudocapacitive materials is the prerequisite for scientifically valid performance evaluations and comparisons, as the mechanisms on performance degradation and corresponding resolutions could differ fundamentally based on the nature of electrode materials.

TABLE 1 Failure modes and corresponding solutions of the pseudocapacitive materials presented in this article

Material	Reason of failure	Strategy	Representative work	Capacitance retention (testing conditions)
Conjugated polymers	Structure pulverization	Spatial confinement	PPy films confined in $Ti_3C_2T_x$ nanosheets[99]	~92% (100 mV s^{-1}, 25 000 cycles, 1 M H_2SO_4 [aq])
		Surface coating	Carbonaceous coated PANI and PPy nanowires[103]	PANI: ~95% PPy: ~85% (100 mV s^{-1}, 10 000 cycles, 1 M H_2SO_4 [aq])
		Nanostructuring	PEDOT/PEO interpenetrating networks[109]	97.5% (10 A g^{-1}, 3000 cycles, 1 M $LiClO_4$ (organic)]
		Molecular structure ordering	Pseudolayered PPy film[32]	~50% (3 A g^{-1}, 230 000 cycles, PVA/H_3PO_4 gel electrolyte]
	Counterion drain effect	Immobile counterion doping	β-naphthalene sulfonate doped PPy films[49]	97% (50 mV s^{-1}, 10 000 cycles, 3 M KCl [aq])
Metal oxide	Structure pulverization	Building carbon-based composites	Graphene foam/CNT/Fe_2O_3 nanoparticle[120]	86.2% (20 mA cm^{-2}, 50 000 cycles, 2 M KOH [aq])
		Nanostructuring	NiO decorated $NiCo_2O_4$ nanoneedles and nanoslices[144]	100% (both) (8 mA cm^{-2}, 12 000 cycles, 6 M KOH [aq])
		Gel electrolytes	PMMA/acetonitrile for δ-MnO_2 (143 nm-thick) nanosheets[33]	100% (100 mV s^{-1}, 200 000 cycles, $LiClO_4$ PMMA/acetonitrile gel)
		Ion preinsertion	Hydrated zinc ion-intercalated δ-MnO_2 nanosheets[36]	100% (5 A g^{-1}, 20 000 cycles, 1 M Na_2SO_4 [aq])
	Dissolution	Tuning valence state	V^{4+}-enriched V_2O_5 nanowires[119]	~70% (60 mA cm^{-2}, 10 000 cycles, 5 M LiCl [aq])
		Gel electrolytes	PVA/LiCl for vanadium oxide nanowires[62]	~85% (100 mV s^{-1}, 5000 cycles, PVA/LiCl gel)
Metal nitride and carbide	Oxidation	Surface coating	Carbon-coated TiN nanowires[41]	~92% (15 000 cycles, 100 mV s^{-1}, 1 M KOH [aq])
		Gel electrolytes	PVA/KOH for TiN nanowires[42]	83% (100 mV s^{-1}, 15 000 cycles, PVA/KOH gel]
		Cation intercalation	Na^+-intercalated V_2CT_x films[168]	100% (10 A g^{-1}, 10 000 cycles, 5 M LiCl [aq])
Metal sulfide	Structural pulverization	Forming composites	N-doped graphene-wrapped Co_8FeS_8 nanoparticles[170]	96.1% (20 A g^{-1}, 10 000 cycles, 2 M KOH [aq])
		Nanostructuring	Al-doped Co_9S_8 nanosheets on Ni nanotube arrays[203]	94.8% (10 A g^{-1}, 10 000 cycles, 2 M KOH [aq])
			Double-walled hollow NiS nanocubes[189]	93.4% (4 A g^{-1}, 3000 cycles, 3 M KOH [aq])
		Elemental doping	Co^{2+}-doped Ni_3S_4 nanosheets[206]	65.7% (10 000 cycles, 3 M KOH [aq])

Abbreviations: PANI, polyaniline; PEDOT, poly(3,4-ethylenedioxythiopene); PEO, poly(ethylene oxide); PMMA, poly(methyl methacrylate); PPy, polypyrrole; PVA, poly(vinyl alcohol).

Second, supplying cycling stability performance with sufficient experimental conditions is helpful to facilitate performance comparison. These details include cycle number, potential window, scan rate (for CV), current density (for galvanostatic charge-discharge test), potential holding duration (for voltage-hold or potential-

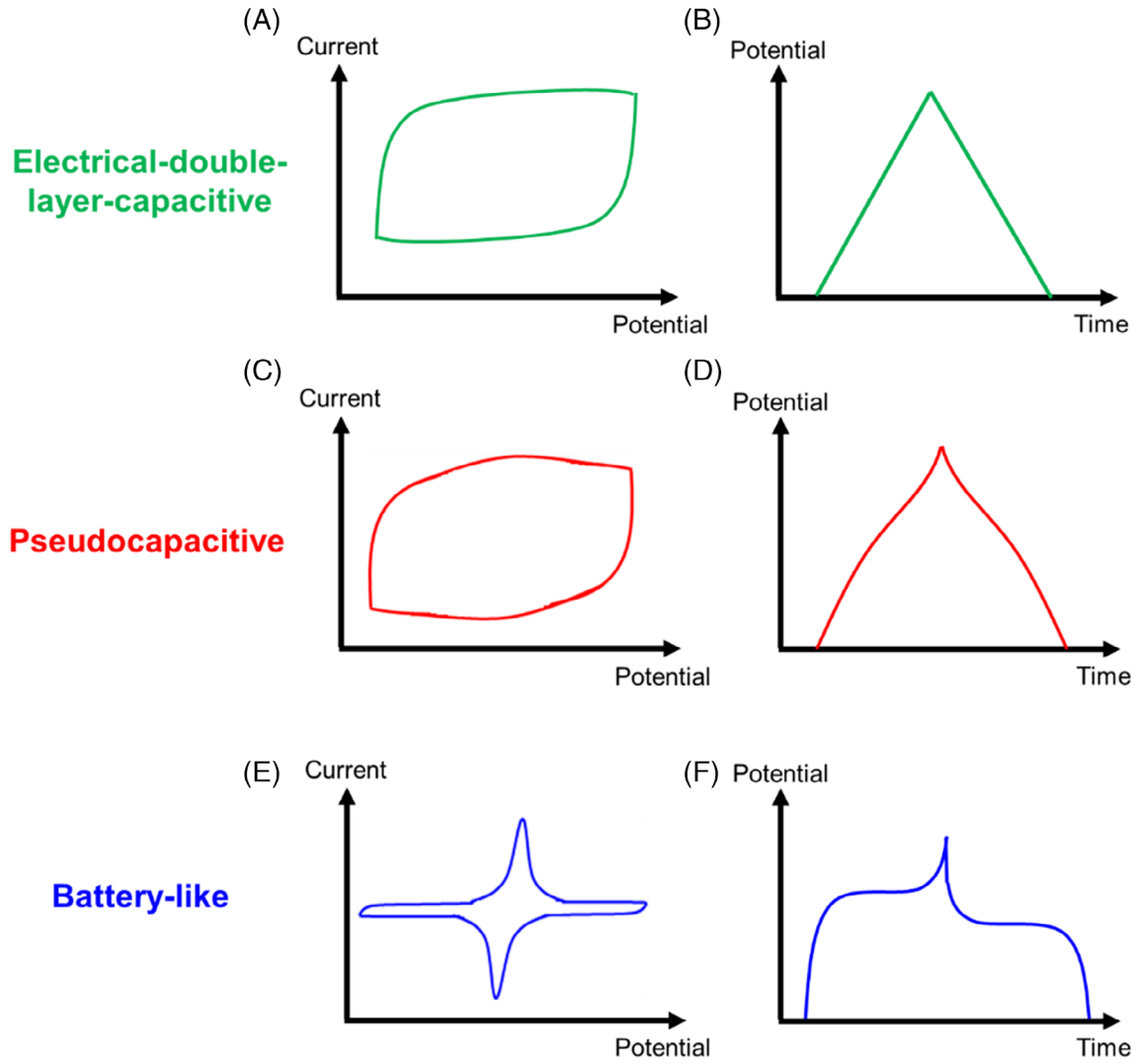

FIGURE 24 Schemes of representative, A,C,E, cyclic voltammograms and, B,D,F, galvanostatic charge–discharge profiles of, A,B, electrical-double-layer capacitive, C,D, pseudocapacitive, and, E,F, battery-like materials

floating method), mass loading, electrolyte composition, and testing temperature. The cycling stability of material could deviate profoundly under different testing conditions. Cycling a material with short durations (eg, <1000 cycles for capacitive materials) could overestimate cycling stability, thus, must be avoided. We are aware that extending cycling tests to the end-of-life for materials of interest might be inapplicable for laboratory evaluations. Therefore, we want to recommend herein the minimum cycles needed for evaluating the cycling stability of supercapacitor electrodes, as proposed by Balducci et al[209]:10 000 cycles and 5000 cycles for electrical double layer capacitive and pseudocapacitive materials, respectively. Extended stability tests are always recommended.

Third, postmortem investigations of the electrodes after cycling are indispensable. Electron microscopy images, XRD, and XPS are useful tools to reveal the evolution in morphology, crystallinity, and composition of the cycled electrode materials, respectively. The obtained information is particularly critical in understanding the origins of capacitance fading, self-activation processes, or stable cycling performance, which offers much more insights than values of capacitance retentions alone, and sometimes might even lead to ground-breaking discoveries. Readers could refer to the postmortem analyses on nanostructured MnO_2 electrodes performed by Chen et al as an excellent example.[143]

Forth, the progress of developing pseudocapacitive materials with outstanding stability calls for interdisciplinary engagements. For example, methods and techniques practiced in battery fields (eg, *operando* electron microscopy)[177,210,211] could also be employed to study

pseudocapacitive materials. Mechanistic insights into intrinsic oxidation resistances of metal-based materials may come from experiences gained in fuel cell and catalysis fields.[212] Industrial developers could guide the stability evaluations of application-oriented devices to facilitate their conversion into commercial products. Close collaborations and conscientious communications across a wide range of disciplines are undoubtedly beneficial to the healthy development of all fields involved.

To sum up, exceptional long-term cycling stability is an essential quality of electrode materials in robust and reliable electrochemical energy storage devices. Achieving this goal is challenging, but consistent, collaborative, and comprehensive efforts will surely make it attainable.

ACKNOWLEDGMENTS

Y.L. thanks the financial support from Merced nAnomaterials Center for Energy and Sensing (MACES), a NASA funded MIRO center, under award NNX15AQ01.

CONFLICT OF INTEREST

The authors declare no conflict of interest.

ORCID

Tianyu Liu https://orcid.org/0000-0002-8716-749X
Yat Li https://orcid.org/0000-0002-8058-2084

REFERENCES

1. Liu L, Zhao H, Lei Y. Advances on three-dimensional electrodes for micro-supercapacitors: a mini-review. *InfoMat*. 2019;1:74-84.
2. Fan X, Liu X, Hu W, Zhong C, Lu J. Advances in the development of power supplies for the internet of everything. *InfoMat*. 2019;1:130-139.
3. Simon P, Gogotsi Y, Dunn B. Where do batteries end and supercapacitors begin? *Science*. 2014;343:1210-1211.
4. Zhang F, Liu TY, Li MY, et al. Multiscale pore network boosts capacitance of carbon electrodes for ultrafast charging. *Nano Lett*. 2017;17:3097-3104.
5. Liu T, Zhang F, Song Y, Li Y. Revitalizing carbon supercapacitor electrodes with hierarchical porous structures. *J Mater Chem A*. 2017;5:17705-17733.
6. Han YQ, Dai LM. Conducting polymers for flexible supercapacitors. *Macromol Chem Phys*. 2019;220:1800355.
7. Wang K, Zhang X, Sun XZ, Ma YW. Conducting polymer hydrogel materials for high-performance flexible solid-state supercapacitors. *Sci China Mater*. 2016;59:412-420.
8. Wang T, Chen HC, Yu F, Zhao XS, Wang HX. Boosting the cycling stability of transition metal compounds-based supercapacitors. *Energy Storage Mater*. 2019;16:545-573.
9. Yu XY, Yu L, Lou XW. Metal sulfide hollow nanostructures for electrochemical energy storage. *Adv Energy Mater*. 2016;6:1501333.
10. Geng PB, Zheng SS, Tang H, et al. Transition metal sulfides based on graphene for electrochemical energy storage. *Adv Energy Mater*. 2018;8:1703259.
11. Balogun MS, Qiu WT, Wang W, Fang PP, Lu XH, Tong YX. Recent advances in metal nitrides as high-performance electrode materials for energy storage devices. *J Mater Chem A*. 2015;3:1364-1387.
12. Zhong Y, Xia XH, Shi F, Zhan JY, Tu JP, Fan HJ. Transition metal carbides and nitrides in energy storage and conversion. *Adv Sci*. 2016;3:1500286.
13. Anasori B, Lukatskaya MR, Gogotsi Y. 2D metal carbides and nitrides (MXenes) for energy storage. *Nat Rev Mater*. 2017;2:16098.
14. Choi C, Ashby DS, Butts DM, et al. Achieving high energy density and high power density with pseudocapacitive materials. *Nat Rev Mater*. 2019;5:5-19.
15. Augustyn V, Simon P, Dunn B. Pseudocapacitive oxide materials for high-rate electrochemical energy storage. *Energ Environ Sci*. 2014;7:1597-1614.
16. Liu T. *Exploration of Carbonaceous Materials for Supercapacitors*. Santa Cruz, CA: Department of Chemistry and Biochemistry, University of California; 2017.
17. Conway BE, Gileadi E. Kinetic theory of pseudo-capacitance and electrode reactions at appreciable surface coverage. *Trans Faraday Soc*. 1962;58:2493-2509.
18. Green CL, Kucernak A. Determination of the platinum and ruthenium surface areas in platinum-ruthenium alloy electrocatalysts by underpotential deposition of copper. I. Unsupported catalysts. *J Phys Chem B*. 2002;106:1036-1047.
19. Augustyn V, Come J, Lowe MA, et al. High-rate electrochemical energy storage through Li^+ intercalation pseudocapacitance. *Nat Mater*. 2013;12:518-522.
20. Marchand R, Brohan L, Tournoux M. TiO_2(B) a new form of titanium-dioxide and the potassium octatitanate $K_2Ti_8O_{17}$. *Mater Res Bull*. 1980;15:1129-1133.
21. Zhu MS, Meng WJ, Huang Y, Huang Y, Zhi CY. Proton-insertion-enhanced pseudocapacitance based on the assembly structure of tungsten oxide. *ACS Appl Mater Interfaces*. 2014;6:18901-18910.
22. Weingarth D, Foelske-Schmitz A, Kötz R. Cycle versus voltage hold—which is the better stability test for electrochemical double layer capacitors? *J Power Sources*. 2013;225:84-88.
23. Weingarth D, Noh H, Foelske-Schmitz A, Wokaun RK. A reliable determination method of stability limits for electrochemical double layer capacitors. *Electrochim Acta*. 2013;103:119-124.
24. Bello A, Barzegar F, Madito MJ, et al. Stability studies of polypyrole- derived carbon based symmetric supercapacitor via potentiostatic floating test. *Electrochim Acta*. 2016;213:107-114.
25. Zhou Z, Liu T, Khan AU, Liu G. Block copolymers based hierarchical porous carbon fibers. *Sci Adv*. 2018;5:eaau6852.
26. Chaari R, Briat O, Deletage JY, Woirgard E, Vinassa JM. How supercapacitors reach end of life criteria during calendar life and power cycling tests. *Microelectron Reliab*. 2011;51:1976-1979.
27. German R, Sari A, Venet P, Briat O, Vinassa JM. Study on specific effects of high frequency ripple currents and temperature on supercapacitors ageing. *Microelectron Reliab*. 2015;55:2027-2031.

28. Bay L, Jacobsen T, Skaarup S, West K. Mechanism of actuation in conducting polymers: osmotic expansion. *J Phys Chem B*. 2001;105:8492-8497.
29. Aydemir N, Kilmartin PA, Travas-Sejdic J, et al. Electrolyte and solvent effects in PPy/DBS linear actuators. *Sensor Actuat B: Chem*. 2015;216:24-32.
30. Maw S, Smela E, Yoshida K, Stein RB. Effects of monomer and electrolyte concentrations on actuation of PPy(DBS) bilayers. *Synth Met*. 2005;155:18-26.
31. Lizarraga L, Andrade EM, Molina FV. Swelling and volume changes of polyaniline upon redox switching. *J Electroanal Chem*. 2004;561:127-135.
32. Huang Y, Zhu MS, Pei ZX, Huang Y, Geng HY, Zhi CY. Extremely stable polypyrrole achieved via molecular ordering for highly flexible supercapacitors. *ACS Appl Mater Interfaces*. 2016;8:2435-2440.
33. Le Thai M, Chandran GT, Dutta RK, Li XW, Penner RM. 100k cycles and beyond: extraordinary cycle stability for MnO_2 nanowires imparted by a gel electrolyte. *ACS Energy Lett*. 2016;1:57-63.
34. Yan WB, Kim JY, Xing WD, Donavan KC, Ayvazian T, Penner RM. Lithographically patterned gold/manganese dioxide core/shell nanowires for high capacity, high rate, and high cyclability hybrid electrical energy storage. *Chem Mater*. 2012; 24:2382-2390.
35. Yan WB, Le Thai M, Dutta R, Li XW, Xing WD, Penner RM. A lithographically patterned capacitor with horizontal nanowires of length 2.5 mm. *ACS Appl Mater Interfaces*. 2014;6:5018-5025.
36. Yao M, Ji X, Chou T-F, et al. Simple and cost-effective approach to dramatically enhance the durability and capability of a layered δ-MnO2 based electrode for pseudocapacitors: a practical electrochemical test and mechanistic revealing. *ACS Appl Energy Mater*. 2019;2:2743-2750.
37. Su Q, Du G, Zhang J, et al. In situ transmission electron microscopy investigation of the electrochemical lithiation-delithiation of individual Co9S8/Co-filled carbon nanotubes. *ACS Nano*. 2013;7:11379-11387.
38. Chyou SD, Shih HC, Chen TT. On the corrosion characterization of titanium nitride in sulfuric-acid-solution. *Corros Sci*. 1993;35:337-347.
39. Choi D, Kumta PN. Nanocrystalline TiN derived by a two-step halide approach for electrochemical capacitors. *J Electrochem Soc*. 2006;153:A2298-A2303.
40. Avasarala B, Haldar P. Electrochemical oxidation behavior of titanium nitride based electrocatalysts under PEM fuel cell conditions. *Electrochim Acta*. 2010;55:9024-9034.
41. Lu XH, Liu TY, Zhai T, et al. Improving the cycling stability of metal-nitride supercapacitor electrodes with a thin carbon shell. *Adv Energy Mater*. 2014;4:1300994.
42. Lu X, Wang G, Zhai T, et al. Stabilized TiN nanowire arrays for high-performance and flexible supercapacitors. *Nano Lett*. 2012;12:5376-5381.
43. Zhang CFJ, Pinilla S, McEyoy N, et al. Oxidation stability of colloidal two-dimensional titanium carbides (MXenes). *Chem Mater*. 2017;29:4848-4856.
44. Lotfi R, Naguib M, Yilmaz DE, Nandab J, Duin ACTV. A comparative study on the oxidation of two-dimensional Ti_3C_2 MXene structures in different environments. *J Mater Chem A*. 2018;6:12733-12743.
45. Habib T, Zhao XF, Shah SA, et al. Oxidation stability of Ti3C2Tx MXene nanosheets in solvents and composite films. *NPJ 2D Mater Appl*. 2019;3:8.
46. Chen W, Wang H, Li Y, et al. In situ electrochemical oxidation tuning of transition metal disulfides to oxides for enhanced water oxidation. *ACS Cent Sci*. 2015;1:244-251.
47. Yan B, Krishnamurthy D, Hendon CH, Deshpande S, Surendranath Y, Viswanathan V. Surface restructuring of nickel sulfide generates optimally coordinated active sites for oxygen reduction catalysis. *Joule*. 2017;1:600-612.
48. Cai X, Song Y, Wang S-Q, Liu XSX-X. Extending the cycle life of high mass loading MoO_x electrode for supercapacitor applications. *Electrochim Acta*. 2019;325:134877.
49. Song Y, Liu TY, Xu XX, Feng DY, Li Y, Liu XX. Pushing the cycling stability limit of polypyrrole for supercapacitors. *Adv Funct Mater*. 2015;25:4626-4632.
50. Le TH, Kim Y, Yoon H. Electrical and electrochemical properties of conducting polymers. *Polymers*. 2017;9:150.
51. Heinze J, Frontana-Uribe BA, Ludwigs S. Electrochemistry of conducting polymers—persistent models and new concepts. *Chem Rev*. 2010;110:4724-4771.
52. Bull RA, Fan FRF, Bard AJ. Polymer-films on electrodes: VII. Electrochemical-behavior at polypyrrole-coated platinum and tantalum electrodes. *J Electrochem Soc*. 1982;129:1009-1015.
53. Beck F, Braun P, Oberst M. Organic electrochemistry in the solid state-overoxidation of polypyrrole. *Phys Chem Chem Phys*. 1987;91:967-974.
54. Krische B, Zagorska M. Overoxidation in conducting polymers. *Synth Met*. 1989;28:C257-C262.
55. Novak P, Rasch B, Vielstich W. Overoxidation of polypyrrole in propylene carbonate—an in situ FTIR study. *J Electrochem Soc*. 1991;138:3300-3304.
56. Lewis TW, Wallace GG, Kim CY, Kim DY. Studies of the overoxidation of polypyrrole. *Synth Met*. 1997;84:403-404.
57. Li YF, Qian RY. Electrochemical overoxidation of conducting polypyrrole nitrate film in aqueous solutions. *Electrochim Acta*. 2000;45:1727-1731.
58. Pang SC, Anderson MA, Chapman TW. Novel electrode materials for thin-film ultracapacitors: comparison of electrochemical properties of sol-gel-derived and electrodeposited manganese dioxide. *J Electrochem Soc*. 2000;147: 444-450.
59. Ataherian F, Lee KT, Wu NL. Long-term electrochemical behaviors of manganese oxide aqueous electrochemical capacitor under reducing potentials. *Electrochim Acta*. 2010;55: 7429-7435.
60. Hsieh Y-C, Lee K-T, Lin Y-P, Wu N-L, Donne S. Investigation on capacity fading of aqueous $MnO_2{\cdot}nH_2O$ electrochemical capacitor. *J Power Sources*. 2008;177:660-664.
61. Nam K-W, Kim MG, Kim K-B. *In situ* Mn K-edge x-ray absorption spectroscopy studies of electrodeposited manganese oxide films for electrochemical capacitors. *J Phys Chem C*. 2007;111:749-758.
62. Wang G, Lu X, Ling Y, et al. LiCl/PVA gel electrolyte stabilizes vanadium oxide nanowire electrodes for pseudocapacitors. *ACS Nano*. 2012;6:10296-10302.
63. Messner M, Walczyk DJ, Palazzo BG, et al. Electrochemical oxidation of metal carbides in aqueous solution. *J Electrochem Soc*. 2018;165:H3107-H3114.

64. Berrueta A, Martin IS, Hernandez A, Ursua A, Sanchis P. Electro-thermal modelling of a supercapacitor and experimental validation. *J Power Sources*. 2014;259:154-165.
65. Wang K, Zhang L, Ji BC, Yuan JL. The thermal analysis on the stackable supercapacitor. *Energy*. 2013;59:440-444.
66. Wang K, Li LW, Yin HX, Zhang TZ, Wan WB. Thermal modelling analysis of spiral wound supercapacitor under constant-current cycling. *PLoS One*. 2015;10:e0138672.
67. Ataherian F, Wu N-L. Long-term charge/discharge cycling stability of MnO_2 aqueous supercapacitor under positive polarization. *J Electrochem Soc*. 2011;158:A422-A427.
68. Mathis TS, Kurra N, Wang X, Pinto D, Simon P, Gogotsi Y. Energy storage data reporting in perspective—guidelines for interpreting the performance of electrochemical energy storage systems. *Adv Energy Mater*. 2019;9:1902007.
69. Zhao YF, Zhang Z, Ren YQ, et al. Vapor deposition polymerization of aniline on 3D hierarchical porous carbon with enhanced cycling stability as supercapacitor electrode. *J Power Sources*. 2015;286:1-9.
70. Wang YC, Tao SY, An YL, Wu S, Meng CG. Bio-inspired high performance electrochemical supercapacitors based on conducting polymer modified coral-like monolithic carbon. *J Mater Chem A*. 2013;1:8876-8887.
71. Fu H, Du ZJ, Zou W, Li HQ, Zhang C. Carbon nanotube reinforced polypyrrole nanowire network as a high-performance supercapacitor electrode. *J Mater Chem A*. 2013; 1:14943-14950.
72. Wu G, Tan PF, Wang DX, et al. High-performance supercapacitors based on electrochemical-induced vertical-aligned carbon nanotubes and polyaniline nanocomposite electrodes. *Sci Rep*. 2017;7:43676.
73. Ye TT, Sun Y, Zhao X, et al. Long-term-stable, solution-processable, electrochromic carbon nanotubes/polymer composite for smart supercapacitor with wide working potential window. *J Mater Chem A*. 2018;6:18994-19003.
74. Zhu YL, Shi KY, Zhitomirsky I. Polypyrrole coated carbon nanotubes for supercapacitor devices with enhanced electrochemical performance. *J Power Sources*. 2014;268:233-239.
75. Tong L, Gao MY, Jiang C, Cai KF. Ultra-high performance and flexible polypyrrole coated CNT paper electrodes for all-solid-state supercapacitors. *J Mater Chem A*. 2019;7:10751-10760.
76. Jin L, Jiang Y, Zhang MJ, et al. Oriented polyaniline nanowire arrays grown on dendrimer (PAMAM) functionalized multiwalled carbon nanotubes as supercapacitor electrode materials. *Sci Rep*. 2018;8:6268.
77. Lu XJ, Dou H, Yang SD, et al. Fabrication and electrochemical capacitance of hierarchical graphene/polyaniline/carbon nanotube ternary composite film. *Electrochim Acta*. 2011;56: 9224-9232.
78. Yan J, Wei T, Fan ZJ, et al. Preparation of graphene nanosheet/carbon nanotube/polyaniline composite as electrode material for supercapacitors. *J Power Sources*. 2010;195:3041-3045.
79. Zhu ZZ, Wang GC, Sun MQ, Li XW, Li CZ. Fabrication and electrochemical characterization of polyaniline nanorods modified with sulfonated carbon nanotubes for supercapacitor applications. *Electrochim Acta*. 2011;56:1366-1372.
80. Liu XB, Shang PB, Zhang YB, et al. Three-dimensional and stable polyaniline-grafted graphene hybrid materials for supercapacitor electrodes. *J Mater Chem A*. 2014;2:15273-15278.
81. Shao F, Bian SW, Zhu Q, Guo MX, Liu S, Peng YH. Fabrication of polyaniline/graphene/polyester textile electrode materials for flexible supercapacitors with high capacitance and cycling stability. *Chem-Asian J*. 2016;11:1906-1912.
82. Song Y, Xu JL, Liu XX. Electrochemical anchoring of dual doping polypyrrole on graphene sheets partially exfoliated from graphite foil for high-performance supercapacitor electrode. *J Power Sources*. 2014;249:48-58.
83. Li JP, Xiao DS, Ren YQ, Liu HR, Chen ZX, Xiao JM. Bridging of adjacent graphene/polyaniline layers with polyaniline nanofibers for supercapacitor electrode materials. *Electrochim Acta*. 2019;300:193-201.
84. Zhang JT, Zhao XS. Conducting polymers directly coated on reduced graphene oxide sheets as high-performance supercapacitor electrodes. *J Phys Chem C*. 2012;116:5420-5426.
85. Zhang K, Zhang LL, Zhao XS, Wu JS. Graphene/polyaniline nanofiber composites as supercapacitor electrodes. *Chem Mater*. 2010;22:1392-1401.
86. Xu JJ, Wang K, Zu SZ, Han BH, Wei ZX. Hierarchical nanocomposites of polyaniline nanowire arrays on graphene oxide sheets with synergistic effect for energy storage. *ACS Nano*. 2010;4:5019-5026.
87. Yang C, Zhang LL, Hu NT, et al. Rational design of sandwiched polyaniline nanotube/layered graphene/polyaniline nanotube papers for high-volumetric supercapacitors. *Chem Eng J*. 2017;309:89-97.
88. Yang C, Zhang LL, Hu NT, Yang Z, Wei H, Zhang YF. Reduced graphene oxide/polypyrrole nanotube papers for flexible all-solid-state supercapacitors with excellent rate capability and high energy density. *J Power Sources*. 2016;302:39-45.
89. Tayel MB, Soliman MM, Ebrahim S, Harb ME. Sprayed polyaniline layer onto chemically reduced graphene oxide as electrode for high performance supercapacitor. *Synth Met*. 2016; 217:237-243.
90. Ma C, Cao WT, Xin W, Bian J, Ma MG. Flexible and free-standing reduced graphene oxide and polypyrrole coated air-laid paper-based supercapacitor electrodes. *Ind Eng Chem Res*. 2019;58:12018-12027.
91. Ni T, Xu L, Sun YP, Yao W, Dai TY, Lu Y. Facile fabrication of reduced graphene oxide/polypyrrole composite hydrogels with excellent electrochemical performance and compression capacity. *ACS Sustain Chem Eng*. 2015;3:862-870.
92. Hu F, Li WH, Zhang J, Meng W. Effect of graphene oxide as a dopant on the electrochemical performance of graphene oxide/polyaniline composite. *J Mater Sci Technol*. 2014;30:321-327.
93. Huang LP, Rao WD, Fan LL, et al. Paper electrodes coated with partially-exfoliated graphite and polypyrrole for high-performance flexible supercapacitors. *Polymers*. 2018;10:135.
94. Cheng Q, Tang J, Ma J, Zhang H, Shinya N, Qin LC. Polyaniline-coated electro-etched carbon fiber cloth electrodes for supercapacitors. *J Phys Chem C*. 2011;115:23584-23590.
95. Lyu SY, Chen YP, Han SJ, et al. Layer-by-layer assembled polyaniline/carbon nanomaterial-coated cellulosic aerogel electrodes for high-capacitance supercapacitor applications. *RSC Adv*. 2018;8:13191-13199.
96. Tang HJ, Wang JY, Yin HJ, Zhao HJ, Wang D, Tang ZY. Growth of polypyrrole ultrathin films on MoS_2 monolayers as high-performance supercapacitor electrodes. *Adv Mater*. 2015; 27:1117-1123.

97. Ma GF, Peng H, Mu JJ, Huang HH, Zhou XZ, Lei ZQ. In situ intercalative polymerization of pyrrole in graphene analogue of MoS_2 as advanced electrode material in supercapacitor. *J Power Sources*. 2013;229:72-78.
98. Luo SJ, Zhao JL, Zou JF, et al. Self-standing polypyrrole/black phosphorus laminated film: promising electrode for flexible supercapacitor with enhanced capacitance and cycling stability. *ACS Appl Mater Interfaces*. 2018;10:3538-3548.
99. Boota M, Anasori B, Voigt C, Zhao MQ, Barsoum MW, Gogotsi Y. Pseudocapacitive electrodes produced by oxidant-free polymerization of pyrrole between the layers of 2D titanium carbide (MXene). *Adv Mater*. 2016;28:1517-1522.
100. Xia C, Chen W, Wang XB, Hedhili MN, Wei NN, Alshareef HN. Highly stable supercapacitors with conducting polymer core-shell electrodes for energy storage applications. *Adv Energy Mater*. 2015;5:1401805.
101. Xie KY, Li J, Lai YQ, et al. Polyaniline nanowire array encapsulated in titania nanotubes as a superior electrode for supercapacitors. *Nanoscale*. 2011;3:2202-2207.
102. Kim BC, Kwon JS, Ko JM, Park JH, Too CO, Wallace GG. Preparation and enhanced stability of flexible supercapacitor prepared from Nafion/polyaniline nanofiber. *Synth Met*. 2010; 160:94-98.
103. Liu TY, Finn L, Yu MH, et al. Polyaniline and polypyrrole pseudocapacitor electrodes with excellent cycling stability. *Nano Lett*. 2014;14:2522-2527.
104. Khosrozadeh A, Singh G, Wang Q, Luo GX, Xing M. Supercapacitor with extraordinary cycling stability and high rate from nano-architectured polyaniline/graphene on Janus nanofibrous film with shape memory. *J Mater Chem A*. 2018; 6:21064-21077.
105. Huang JY, Wang K, Wei ZX. Conducting polymer nanowire arrays with enhanced electrochemical performance. *J Mater Chem*. 2010;20:1117-1121.
106. Xu WB, Mu B, Zhang WB, Wang AQ. Facile fabrication of well-defined polyaniline microtubes derived from natural kapok fibers for supercapacitors with long-term cycling stability. *RSC Adv*. 2016;6:68302-68311.
107. Shi Y, Pan LJ, Liu BR, et al. Nanostructured conductive polypyrrole hydrogels as high-performance, flexible supercapacitor electrodes. *J Mater Chem A*. 2014;2:6086-6091.
108. Zhao Y, Liu BR, Pan LJ, Yu GH. 3D nanostructured conductive polymer hydrogels for high-performance electrochemical devices. *Energ Environ Sci*. 2013;6:2856-2870.
109. Fong KD, Wang T, Kim HK, Kumar RV, Smoukov SK. Semi-interpenetrating polymer networks for enhanced supercapacitor electrodes. *ACS Energy Lett*. 2017;2:2014-2020.
110. Huang L, Yao X, Yuan LY, et al. 4-Butylbenzenesulfonate modified polypyrrole paper for supercapacitor with exceptional cycling stability. *Energy Storage Mater*. 2018;12: 191-196.
111. Chen S, Zhitomirsky I. Polypyrrole electrodes doped with sulfanilic acid azochromotrop for electrochemical supercapacitors. *J Power Sources*. 2013;243:865-871.
112. Kumar A, Singh RK, Singh HK, Srivastava P, Singh R. Enhanced capacitance and stability of p-toluenesulfonate doped polypyrrole/carbon composite for electrode application in electrochemical capacitors. *J Power Sources*. 2014;246: 800-807.
113. Chen GF, Li XX, Zhang LY, Li N, Ma TY, Liu ZQ. A porous perchlorate-doped polypyrrole nanocoating on nickel nanotube arrays for stable wide-potential-window supercapacitors. *Adv Mater*. 2016;28:7680-7687.
114. Shi KY, Zhitomirsky I. Influence of current collector on capacitive behavior and cycling stability of Tiron doped polypyrrole electrodes. *J Power Sources*. 2013;240:42-49.
115. Vonlanthen D, Lazarev P, See KA, Wudl F, Heeger AJ. A Stable Polyaniline-Benzoquinone-Hydroquinone Supercapacitor. *Adv Mater*. 2014;26:5095-5100.
116. Ren LJ, Zhang GN, Lei J, Wang Y, Hu DW. Novel layered polyaniline-poly(hydroquinone)/graphene film as supercapacitor electrode with enhanced rate performance and cycling stability. *J Colloid Interface Sci*. 2018;512:300-307.
117. Zhu YR, Ji XB, Pan CC, et al. A carbon quantum dot decorated RuO_2 network: outstanding supercapacitances under ultrafast charge and discharge. *Energ Environ Sci*. 2013;6: 3665-3675.
118. Prasath A, Athika M, Duraisamy E, Sharma AS, Devi VS, Elumalai P. Carbon quantum dot-anchored bismuth oxide composites as potential electrode for lithium-ion battery and supercapacitor applications. *ACS Omega*. 2019;4:4943-4954.
119. Song Y, Liu T-Y, Yao B, et al. Amorphous mixed-valence vanadium oxide/exfoliated carbon cloth structure shows a record high cycling stability. *Small*. 2017;13:1700067.
120. Guan C, Liu JL, Wang YD, et al. Iron oxide-decorated carbon for supercapacitor anodes with ultrahigh energy density and outstanding cycling stability. *ACS Nano*. 2015;9:5198-5207.
121. Pandit B, Dubal DP, Gomez-Romero P, Kale BB, Sankapal BR. V_2O_5 encapsulated MWCNTs in 2D surface architecture: complete solid-state bendable highly stabilized energy efficient supercapacitor device. *Sci Rep*. 2017;7:43430.
122. Boukhalfa S, Evanoff K, Yushin G. Atomic layer deposition of vanadium oxide on carbon nanotubes for high-power supercapacitor electrodes. *Energ Environ Sci*. 2012;5:6872-6879.
123. Wang X, Han XD, Lim M, et al. Nickel cobalt oxide-single wall carbon nanotube composite material for superior cycling stability and high-performance supercapacitor application. *J Phys Chem C*. 2012;116:12448-12454.
124. Li L, Hu ZA, An N, Yang YY, Li ZM, Wu HY. Facile synthesis of MnO_2/CNTs composite for supercapacitor electrodes with long cycle stability. *J Phys Chem C*. 2014;118:22865-22872.
125. Lee TH, Pham DT, Sahoo R, Seok J, Luu THT, Lee YH. High energy density and enhanced stability of asymmetric supercapacitors with mesoporous MnO2@CNT and nanodot MoO3@CNT free-standing films. *Energy Storage Mater*. 2018; 12:223-231.
126. Guan C, Qian X, Wang X, et al. Atomic layer deposition of Co_3O_4 on carbon nanotubes/carbon cloth for highcapacitance and ultrastable supercapacitor electrode. *Nanotechnology*. 2015;26:094001.
127. Lee JW, Hall AS, Kim JD, Mallouk TE. A facile and template-free hydrothermal synthesis of Mn_3O_4 nanorods on graphene sheets for supercapacitor electrodes with long cycle stability. *Chem Mater*. 2012;24:1158-1164.
128. Song Y, Feng DY, Liu TY, Li Y, Liu XX. Controlled partial-exfoliation of graphite foil and integration with MnO_2 nanosheets for electrochemical capacitors. *Nanoscale*. 2015;7: 3581-3587.

129. Li ZP, Mi YJ, Liu XH, Liu S, Yang SR, Wang JQ. Flexible graphene/MnO_2 composite papers for supercapacitor electrodes. *J Mater Chem*. 2011;21:14706-14711.
130. Yu XZ, Lu BG, Xu Z. Super long-life supercapacitors based on the construction of nanohoneycomb-like strongly coupled $CoMoO_4$-3D graphene hybrid electrodes. *Adv Mater*. 2014;26:990-990.
131. Zhou K, Zhou W, Liu X, et al. Ultrathin MoO_3 nanocrystals self-assembled on graphene nanosheets via oxygen bonding as supercapacitor electrodes of high capacitance and long cycle life. *Nano Energy*. 2015;12:510-520.
132. Chodankar NR, Dubal DP, Ji SH, Kim DH. Highly efficient and stable negative electrode for asymmetric supercapacitors based on graphene/FeCo2O4 nanocomposite hybrid material. *Electrochim Acta*. 2019;295:195-203.
133. Qu QT, Yang SB, Feng XL. 2D sandwich-like sheets of iron oxide grown on graphene as high energy anode material for supercapacitors. *Adv Mater*. 2011;23:5574-5580.
134. Mao L, Zhang K, Chan HSO, Wu JS. Nanostructured MnO_2/graphene composites for supercapacitor electrodes: the effect of morphology, crystallinity and composition. *J Mater Chem*. 2012;22:1845-1851.
135. Ma HN, He J, Xiong DB, et al. Nickel cobalt hydroxide@reduced graphene oxide hybrid nanolayers for high performance asymmetric supercapacitors with remarkable cycling stability. *ACS Appl Mater Interfaces*. 2016;8:1992-2000.
136. Oh KH, Gund GS, Park HS. Stabilizing $NiCo_2O_4$ hybrid architectures by reduced graphene oxide interlayers for improved cycling stability of hybrid supercapacitors. *J Mater Chem A*. 2018;6:22106-22114.
137. Zhao YF, Ran W, He J, et al. High-performance asymmetric supercapacitors based on multilayer MnO_2/graphene oxide nanoflakes and hierarchical porous carbon with enhanced cycling stability. *Small*. 2015;11:1310-1319.
138. Li RZ, Wang YM, Zhou C, et al. Carbon-stabilized high-capacity ferroferric oxide nanorod array for flexible solid-state alkaline battery-supercapacitor hybrid device with high environmental suitability. *Adv Funct Mater*. 2015;25:5384-5394.
139. Ouyang Y, Xia XF, Ye HT, et al. Three-dimensional hierarchical structure ZnO@C@NiO on carbon cloth for asymmetric supercapacitor with enhanced cycle stability. *ACS Appl Mater Interfaces*. 2018;10:3549-3561.
140. Peng X, Huo KF, Fu JJ, et al. Porous dual-layered MoO_x nanotube arrays with highly conductive TiN cores for supercapacitors. *ChemElectroChem*. 2015;2:512-517.
141. Yu L, Zhang GQ, Yuan CZ, Lou XW. Hierarchical $NiCo_2O_4$@MnO_2 core-shell heterostructured nanowire arrays on Ni foam as high-performance supercapacitor electrodes. *Chem Commun*. 2013;49:137-139.
142. Lu L, Xie YB, Zhao ZC. Improved electrochemical stability of $Ni_xCo_{2x}(OH)_{6x}$/$NiCo_2O_4$ electrode material. *J Alloy Compd*. 2018;731:903-913.
143. Chen W, Rakhi RB, Wang QX, Hedhili MN, Alshareef HN. Morphological and electrochemical cycling effects in MnO_2 nanostructures by 3D electron tomography. *Adv Funct Mater*. 2014;24:3130-3143.
144. Ouyang Y, Huang RJ, Xia XF, et al. Hierarchical structure electrodes of NiO ultrathin nanosheets anchored to $NiCo_2O_4$ on carbon cloth with excellent cycle stability for asymmetric supercapacitors. *Chem Eng J*. 2019;355:416-427.
145. Wu C, Zhu Y, Ding M, Jia CK, Zhang KL. Fabrication of plate-like MnO_2 with excellent cycle stability for supercapacitor electrodes. *Electrochim Acta*. 2018;291:249-255.
146. Cui MJ, Tang SC, Ma YJ, Shi XL, Syed JA, Meng XK. Monolayer standing MnO_2-Nanosheet covered Mn_3O_4 octahedrons anchored in 3D N-doped graphene networks as supercapacitor electrodes with remarkable cycling stability. *J Power Sources*. 2018;396:483-490.
147. Ma Z, Shao G, Fan Y, Wang G, Song J, Shen D. Construction of hierarchical α-MnO_2 nanowires@ultrathin δ-MnO2 nanosheets core−shell nanostructure with excellent cycling stability for high-power asymmetric supercapacitor electrodes. *ACS Appl Mater Interfaces*. 2016;8:9050-9058.
148. Yu MH, Zhai T, Lu XH, et al. Manganese dioxide nanorod arrays on carbon fabric for flexible solid-state supercapacitors. *J Power Sources*. 2013;239:64-71.
149. Yu MH, Zeng Y, Han Y, et al. Valence-optimized vanadium oxide supercapacitor electrodes exhibit ultrahigh capacitance and super-long cyclic durability of 100 000 cycles. *Adv Funct Mater*. 2015;25:3534-3540.
150. Yu DM, Zhang ST, Liu DW, et al. Effect of manganese doping on Li-ion intercalation properties of V_2O_5 films. *J Mater Chem*. 2010;20:10841-10846.
151. Dong R, Song Y, Yang D, et al. Electrochemical in situ construction of vanadium oxide heterostructures with boosted pseudocapacitive charge storage. *J Mater Chem A*. 2020;8:1176-1183.
152. Engstrom AM, Doyle FM. Exploring the cycle behavior of electrodeposited vanadium oxide electrochemical capacitor electrodes in various aqueous environments. *J Power Sources*. 2013;228:120-131.
153. Gao B, Li XX, Guo XL, et al. Nitrogen-doped carbon encapsulated mesoporous vanadium nitride nanowires as self-supported electrodes for flexible all-solid-state supercapacitors. *Adv Mater Interfaces*. 2015;2:1500211.
154. An GH, Lee DY, Ahn HJ. Vanadium nitride encapsulated carbon fibre networks with furrowed porous surfaces for ultrafast asymmetric supercapacitors with robust cycle life. *J Mater Chem A*. 2017;5:19714-19720.
155. Grote F, Zhao HP, Lei Y. Self-supported carbon coated TiN nanotube arrays: innovative carbon coating leads to an improved cycling ability for supercapacitor applications. *J Mater Chem A*. 2015;3:3465-3470.
156. Balamurugan J, Nguyen TT, Aravindan V, Kim NH, Lee JH. Flexible solid-state asymmetric supercapacitors based on nitrogen-doped graphene encapsulated ternary metal-nitrides with ultralong cycle life. *Adv Funct Mater*. 2018;28:1804663.
157. Tian F, Xie YB, Du HX, Zhou YZ, Xia C, Wang W. Preparation and electrochemical capacitance of graphene/titanium nitride nanotube array. *RSC Adv*. 2014;4:41856-41863.
158. He TQ, Wang Z, Li XM, et al. Intercalation structure of vanadium nitride nanoparticles growing on graphene surface toward high negative active material for supercapacitor utilization. *J Alloy Compd*. 2019;781:1054-1058.
159. Balamurugan J, Karthikeyan G, Thanh TD, Kim NH, Lee JH. Facile synthesis of vanadium nitride/nitrogen-doped graphene

composite as stable high performance anode materials for supercapacitors. *J Power Sources*. 2016;308:149-157.
160. Xia C, Xie YB, Wang Y, Wang W, Du HX, Tian F. Preparation and capacitance performance of polyaniline/titanium nitride nanotube hybrid. *J Appl Electrochem*. 2013;43:1225-1233.
161. Xie YB, Du HX, Xia C. Porous poly(3,-4-ethylenedioxythiophene) nanoarray used for flexible supercapacitor. *Micropor Mesopor Mater*. 2015;204:163-172.
162. Wang HY, Li B, Teng JX, et al. N-doped carbon-coated TiN exhibiting excellent electrochemical performance for supercapacitors. *Electrochim Acta*. 2017;257:56-63.
163. Wang ZQ, Li ZS, Feng JY, et al. MnO_2 nanolayers on highly conductive $TiO_{0.54}N_{0.46}$ nanotubes for supercapacitor electrodes with high power density and cyclic stability. *Phys Chem Chem Phys*. 2014;16:8521-8528.
164. Zhu CR, Yang PH, Chao DL, et al. All metal nitrides solid-state symmetric supercapacitors. *Adv Mater*. 2015;27:4566-4571.
165. Wang PY, Wang RT, Lang JW, Zhang X, Chen ZK, Yan XB. Porous niobium nitride as a capacitive anode material for advanced Li-ion hybrid capacitors with superior cycling stability. *J Mater Chem A*. 2016;4:9760-9766.
166. Achour A, Ducros JB, Porto RL, et al. Hierarchical nanocomposite electrodes based on titanium nitride and carbon nanotubes for micro-supercapacitors. *Nano Energy*. 2014;7:104-113.
167. Yao B, Li M, Zhang J, et al. TiN paper for ultrafast charging supercapacitors. *Nano-Micro Lett*. 2020;12:3.
168. VahidMohammadi A, Mojtabavi M, Caffrey NM, Wanunu M, Beidaghi M. Assembling 2D MXenes into highly stable pseudocapacitive electrodes with high power and energy densities. *Adv Mater*. 2019;31:1806931.
169. De B, Kuila T, Kim NH, Lee JH. Carbon dot stabilized copper sulphide nanoparticles decorated graphene oxide hydrogel for high performance asymmetric supercapacitor. *Carbon*. 2017;122:247-257.
170. Al Haj Y, Balamurugan J, Kim NH, Lee JH. Nitrogen-doped graphene encapsulated cobalt iron sulfide as an advanced electrode for high-performance asymmetric supercapacitors. *J Mater Chem A*. 2019;7:3941-3952.
171. Ghosh D, Das CK. Hydrothermal growth of hierarchical Ni_3S_2 and Co_3S_4 on a reduced graphene oxide hydrogel@Ni foam: a high-energy-density aqueous asymmetric supercapacitor. *ACS Appl Mater Interfaces*. 2015;7:1122-1131.
172. Ratha S, Rout CS. Supercapacitor electrodes based on layered tungsten disulfide-reduced graphene oxide hybrids synthesized by a facile hydrothermal method. *ACS Appl Mater Interfaces*. 2013;5:11427-11433.
173. Qu B, Chen Y, Zhang M, et al. β-Cobalt sulfide nanoparticles decorated graphene composite electrodes for high capacity and power supercapacitors. *Nanoscale*. 2012;4:7810-7816.
174. Zhang HM, Yu XZ, Guo D, et al. Synthesis of bacteria promoted reduced graphene oxide-nickel sulfide networks for advanced supercapacitors. *ACS Appl Mater Interfaces*. 2013;5:7335-7340.
175. Wang AM, Wang HL, Zhang SY, et al. Controlled synthesis of nickel sulfide/graphene oxide nanocomposite for high-performance supercapacitor. *Appl Surf Sci*. 2013;282:704-708.
176. Zhang QF, Xu CM, Lu BG. Super-long life supercapacitors based on the construction of Ni foam/graphene/Co_3S_4 composite film hybrid electrodes. *Electrochim Acta*. 2014;132:180-185.
177. Zhao FP, Gong QF, Traynor B, et al. Stabilizing nickel sulfide nanoparticles with an ultrathin carbon layer for improved cycling performance in sodium ion batteries. *Nano Res*. 2016;9:3162-3170.
178. Hou XY, Liu XM, Lu Y, et al. Copper sulfide nanoneedles on CNT backbone composite electrodes for high-performance supercapacitors and Li-S batteries. *J Solid State Electrochem*. 2017;21:349-359.
179. Wang QH, Jiao LF, Du HM, Si YC, Wang YJ, Yuan HT. Co_3S_4 hollow nanospheres grown on graphene as advanced electrode materials for supercapacitors. *J Mater Chem*. 2012;22:21387-21391.
180. Dai CS, Chien PY, Lin JY, et al. Hierarchically structured Ni_3S_2/carbon nanotube composites as high performance cathode materials for asymmetric supercapacitors. *ACS Appl Mater Interfaces*. 2013;5:12168-12174.
181. Kumuthini R, Ramachandran R, Therese HA, Wang F. Electrochemical properties of electrospun MoS_2@C nanofiber as electrode material for high-performance supercapacitor application. *J Alloy Compd*. 2017;705:624-630.
182. Li LL, Ding YH, Huang HJ, et al. Controlled synthesis of unique Co_9S_8 nanostructures with carbon coating as advanced electrode for solid-state asymmetric supercapacitors. *J Colloid Interface Sci*. 2019;540:389-397.
183. Liang X, Nie KW, Ding X, et al. Highly compressible carbon sponge supercapacitor electrode with enhanced performance by growing nickel-cobalt sulfide nanosheets. *ACS Appl Mater Interfaces*. 2018;10:10087-10095.
184. Zuo LZ, Fan W, Zhang YF, Huang YP, Gao W, Liu TX. Bacterial cellulose-based sheet-like carbon aerogels for the in situ growth of nickel sulfide as high performance electrode materials for asymmetric supercapacitors. *Nanoscale*. 2017;9:4445-4455.
185. Shen LF, Wang J, Xu GY, Li HS, Dou H, Zhang XG. $NiCo_2S_4$ nanosheets grown on nitrogen-doped carbon foams as an advanced electrode for supercapacitors. *Adv Energy Mater*. 2015;5:1400977.
186. Zhang YF, Zuo LZ, Zhang LS, et al. Immobilization of NiS nanoparticles on N-doped carbon fiber aerogels as advanced electrode materials for supercapacitors. *Nano Res*. 2016;9:2747-2759.
187. Huang YY, Shi TL, Jiang SL, et al. Enhanced cycling stability of $NiCo_2S_4$@NiO core-shell nanowire arrays for all-solid-state asymmetric supercapacitors. *Sci Rep*. 2016;6:38620.
188. Liang MM, Zhao MS, Wang HY, Zheng QY, Song XP. Superior cycling stability of a crystalline/amorphous Co_3S_4 core-shell heterostructure for aqueous hybrid supercapacitors. *J Mater Chem A*. 2018;6:21350-21359.
189. Yu X-Y, Yu L, Shen L, Song X, Chen H, Lou XWD. General formation of MS (M = Ni, Cu, Mn) box-in-box hollow structures with enhanced pseudocapacitive properties. *Adv Funct Mater*. 2014;224:7440-7446.
190. Wei CZ, Chen QY, Cheng C, Liu R, Zhang Q, Zhang LP. Mesoporous nickel cobalt manganese sulfide yolk-shell hollow spheres for high-performance electrochemical energy storage. *Inorg Chem Front*. 2019;6:1851-1860.
191. Harish S, Naveen AN, Abinaya R, et al. Enhanced performance on capacity retention of hierarchical NiS hexagonal

nanoplate for highly stable asymmetric supercapacitor. *Electrochim Acta*. 2018;283:1053-1062.
192. Zha DS, Fu YS, Zhang LL, Zhu JW, Wang X. Design and fabrication of highly open nickel cobalt sulfide nanosheets on Ni foam for asymmetric supercapacitors with high energy density and long cycle-life. *J Power Sources*. 2018;378:31-39.
193. Han X, Tao K, Wang D, Han L. Design of a porous cobalt sulfide nanosheet array on Ni foam from zeolitic imidazolate frameworks as an advanced electrode for supercapacitors. *Nanoscale*. 2018;10:2735-2741.
194. Li XM, Li QG, Wu Y, Rui MC, Zeng HB. Two-dimensional, porous nickel cobalt sulfide for high-performance asymmetric supercapacitors. *ACS Appl Mater Interfaces*. 2015;7:19316-19323.
195. Yang ZS, Chen CY, Chang HT. Supercapacitors incorporating hollow cobalt sulfide hexagonal nanosheets. *J Power Sources*. 2011;196:7874-7877.
196. Patil SJ, Kim JH, Lee DW. Self-assembled Ni_3S_2//$CoNi_2S_4$ nanoarrays for ultra high-performance supercapacitor. *Chem Eng J*. 2017;322:498-509.
197. Li YH, Liu H, Xu J, et al. Hierarchical nanostructure-tuned super-high electrochemical stability of nickel cobalt sulfide. *J Mater Chem A*. 2018;6:19788-19797.
198. Zhang ZM, Wang Q, Zhao CJ, Min SD, Qian XZ. One-step hydrothermal synthesis of 3D petal-like Co_9S_8/RGO/Ni_3S_2 composite on nickel foam for high-performance supercapacitors. *ACS Appl Mater Interfaces*. 2015;7:4861-4868.
199. Wen YX, Peng SL, Wang ZL, et al. Facile synthesis of ultrathin $NiCo_2S_4$ nano-petals inspired by blooming buds for high-performance supercapacitors. *J Mater Chem A*. 2017;5:7144-7152.
200. Xia XH, Zhu CR, Luo JS, et al. Synthesis of free-standing metal sulfide nanoarrays via anion exchange reaction and their electrochemical energy storage application. *Small*. 2014;10:766-773.
201. Li H, Yue F, Xie HT, et al. Hollow shell-in-shell Ni_3S_4@Co_9S_8 tubes derived from core-shell Ni-MOF-74@co-MOF-74 as efficient faradaic electrodes. *CrstEngComm*. 2018;20:889-895.
202. Kong W, Lu CC, Zhang W, Pu J, Wang ZH. Homogeneous core-shell $NiCo_2S_4$ nanostructures supported on nickel foam for supercapacitors. *J Mater Chem A*. 2015;3:12452-12460.
203. Huang J, Wei JC, Xiao YB, et al. When Al-doped cobalt sulfide nanosheets meet nickel nanotube arrays: a highly efficient and stable cathode for asymmetric supercapacitors. *ACS Nano*. 2018;12:3030-3041.
204. Chen Q, Li HX, Cai CY, et al. In situ shape and phase transformation synthesis of Co_3S_4 nanosheet arrays for high-performance electrochemical supercapacitors. *RSC Adv*. 2013;3:22922-22926.
205. Xin BB, Zhao YQ, Xu CL. A high mass loading electrode based on ultrathin Co_3S_4 nanosheets for high performance supercapacitor. *J Solid State Electrochem*. 2016;20:2197-2205.
206. Li YH, Li J, Wang M, Liu YY, Cui HT. High rate performance and stabilized cycle life of Co^{2+}-doped nickel sulfide nanosheets synthesized by a scalable method of solid-state reaction. *Chem Eng J*. 2019;366:33-40.
207. Brousse T, Bélanger D, Long JW. To be or not to be pseudocapacitive? *J Electrochem Soc*. 2015;162:A5185-A5189.
208. Xie J, Yang P, Wang Y, Qi T, Lei Y, Li CM. Puzzles and confusions in supercapacitor and battery: theory and solutions. *J Power Sources*. 2018;401:213-223.
209. Balducci A, Belanger D, Brousse T, Long JW, Sugimoto W. A guideline for reporting performance metrics with electrochemical capacitors: from electrode materials to full devices. *J Electrochem Soc*. 2017;164:A1487-A1488.
210. Xie D, Yuan YD, Xiao L, et al. Strain redistribution in metal-sulfide-composite anode for enhancing volumetric lithium storage. *ChemElectroChem*. 2018;5:3906-3912.
211. Wang LG, Wang JJ, Guo FM, et al. Understanding the initial irreversibility of metal sulfides for sodium-ion batteries via operando techniques. *Nano Energy*. 2018;43:184-191.
212. Kimmel YC, Xu XG, Yu WT, Yang XD, Chen JGG. Trends in electrochemical stability of transition metal carbides and their potential use as supports for low-cost electrocatalysts. *ACS Catal*. 2014;4:1558-1562.

AUTHOR BIOGRAPHIES

Tianyu Liu currently works as a postdoctoral associate in the Department of Chemistry, Virginia Tech. He obtained his PhD in Chemistry from the University of California, Santa Cruz in 2017, and received his BS degree in Chemistry from the University of Science and Technology, Beijing, China in 2012. His research focuses on the design, synthesis, and evaluation of functional materials in electrochemical energy storage and conversion.

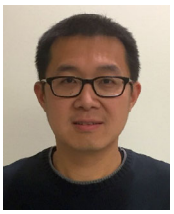

Yat Li received his BSc (1999) and PhD (2002) degrees in Chemistry from The University of Hong Kong. He received postdoctoral training under the supervision of Prof Charles Lieber at Harvard University. He is currently a full professor of chemistry and biochemistry at the University of California, Santa Cruz. His research focuses on the rational design and synthesis of low-dimensional materials, understanding their chemical and physical properties, and realizing their potential applications in catalysis, energy conversion, and storage.

How to cite this article: Liu T, Li Y. Addressing the Achilles' heel of pseudocapacitive materials: Long-term stability. *InfoMat*. 2020;2:807–842. https://doi.org/10.1002/inf2.12105